REVIEW

Aggregate WILEY

Influence of electrolyte structural evolution on battery applications: Cationic aggregation from dilute to high concentration

Jiangtao Hu¹ | Yuchen Ji¹ | Guorui Zheng¹ | Weiyuan Huang¹ | Yuan Lin³ | Luyi Yang¹ | Feng Pan^{1,2} •

- ² Chemistry and Chemical Engineering Guangdong Laboratory, Shantou, People's Republic of China
- ³ Beijing National laboratory for Molecular Sciences, Key Laboratory of Photochemistry, CAS Research/Education Center for Excellence in Molecular Sciences, Institute of Chemistry, Chinese Academy of Sciences, Beijing, People's Republic of China

Correspondence

Guorui Zheng, Luyi Yang, and Feng Pan, School of Advanced Materials, Peking University Shenzhen Graduate School, Shenzhen 518055, People's Republic of China.

Email: zhengguorui1991@163.com; y angly @pkusz.edu.cn; panfeng @pkusz.edu.cn

Funding information

Chemistry and Chemical Engineering Guangdong Laboratory, Grant/Award Number: 1922018; Soft Science Research Project of Guangdong Province, Grant/Award Number: 2017B030301013

Abstract

In the context of the rapid expansion of the electric vehicle market, the request for high-energy-density lithium-ion batteries (LIBs) has steadily increased, hence the demand for highly stable electrolytes. Over the past years, efforts have been devoted to the improvement of electrolyte materials. As a benchmarking breakthrough, the achievement of high concentration electrolyte (HCE) can be attributed to the altered cationic aggregation (i.e., cation-solvent and cation-anion coordination environment), which offers technical superiority over the widely applied conventional dilute electrolytes. More recently, based on the understanding of the dilute electrolyte and HCE, the concept of localized HCE (LHCE) has been proposed and extensively investigated. All these findings reveal a roadmap of electrolyte optimization for high-performance LIBs via coordination structure regulation. Through elucidating the correlation of structure evolution therein and its critical effects on battery performance, this review aims to establish the design principle of electrolytes based on their structures other than component studies and thereby accelerate the development of high-performance electrolytes.

KEYWORDS

cationic aggregate, electrolytes, Li-ion batteries

INTRODUCTION

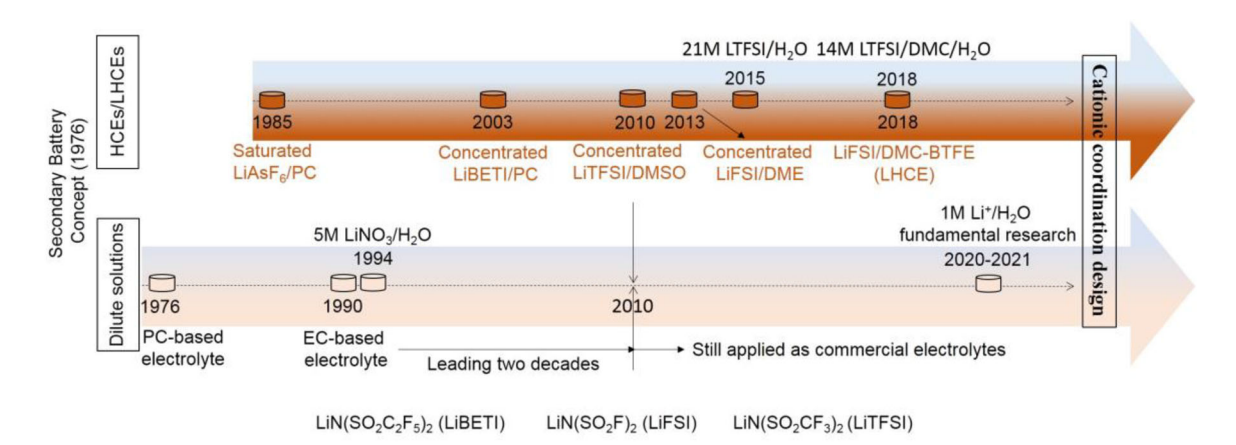
Electrolyte matters and is graphically described as "blood" in rechargeable batteries. This is irrefutable not only for its contribution to promoting fast Li⁺ flow between cathode and anode, but also for stabilizing the electrode/electrolyte interface to avoid its severe damage to the structural integrity of electrode and enable batteries working at extremely active chemical environment and highly operating voltage condition.^[1] In the 1970s, Dr. M. Stanley Whittingham, who was awarded a 2019 Nobel Prize, broke the ground on the first rechargeable battery heralding the advent of the new energy era.^[2] Dahn is the pioneer in the development of battery electrolytes. In 1985, he discovered the co-intercalation issues of propylene carbonate (PC) in graphite anode resulting in the exfoliation of carbon layer^[3] and then designed a new electrolyte with ethylene carbonate (EC) replacement to solve it by repairing graphite/electrolyte interface in 1990.^[4] Based on this critical headway, in 1991, carbonate-based electrolytes were widely applied in lithium-ion batteries (LIBs)^[5] and had deeply permeated into our society, becoming an indispensable part in people's daily life. [6-9] Considering the safety issues induced by the applied organic electrolytes, rechargeable lithium batteries with aqueous electrolytes were presented due to their nonflammability by Dahn et al.[10] From then, aqueous batteries have been included in the hunt for the next generation EV battery.[11-16] Recently, the indicator of high energy density deriving from higher capacity and/or voltage brings new battery race to meet the everimproving requirements.^[17–21] However, the conventional electrolytes with low salt concentration are incompatible for extreme operating potentials when matching high-voltage cathodes and low-voltage anodes for high-energy-density batteries. Therefore, considerable efforts have been made on

This is an open access article under the terms of the Creative Commons Attribution License, which permits use, distribution and reproduction in any medium, provided the original work is properly cited.

© 2022 The Authors. Aggregate published by SCUT, AIEI, and John Wiley & Sons Australia, Ltd.

Aggregate. 2022;3:e153. https://doi.org/10.1002/agt2.153

¹ School of Advanced Materials, Peking University Shenzhen Graduate School, Shenzhen, People's Republic of China



SCHEME 1 Illustration of the development trend of LIB electrolytes

developing new electrolytes. Among them, high concentration electrolytes (HCEs) received more extensive attention, owing to their compatibility with most prevailing electrode materials, wide voltage stability window, [11,22–25] high safety, [26–29] and good current collector protection. [29–31] Following HCEs, the concept of localized HCEs (LHCEs) was developed by Pacific Northwest National Laboratory, which has been used in a wide range of high energy density batteries. [32–35] Nowadays, in different practical applications, different electrolyte systems match their niche to achieve the special requirements, and they are the precious treasure for the future electrolyte selection and design.

It is well acknowledged that the electrochemical performance of battery materials is determined by their structures. Taking electrode materials as an example, [36-41] most of them exhibit crystalline structures consisting of basic structure units (e.g., LiO₄ tetrahedra, LiO₆ octahedra, and TMO₆ octahedra, TM = transitional metal), resulting in vastly different properties through the periodic and unique arrangement. Such fundamental understanding plays an important part in material optimization and new material design. As an equally important component in a battery, electrolyte has received increasing attention due to its huge impact on the battery performance as well (e.g., rate capability, cycle life, and thermal stability).[1,42–48] Nowadays, various optimization approaches, including tuning the choice of solvents, salts, and their ratios, have been developed to fit the requirements of different practical scenarios. If we consider ion-ion and ion-solvent aggregates as structure units of the electrolyte, their interactions will determine the structure of electrolyte, govern the ion transport behavior in the electrolyte and dictate the interface parasitic reaction and the ion interfacial dynamics. Although it has been well demonstrated that electrolyte structure has a significant impact on the electrochemical performance, [11,24,28,33,49] the structure evolution of electrolytes in both bulk and interface is often shrouded in oblivion, resulting in the shortage of comprehensive summary of those seemingly fragmented scientific findings. Hence, it is fulfilling to fill the gap to facilitate the development of high-performance electrolytes.

Here, based on the extensive electrolyte-related works from 1970s to nowadays (as illustrated in Scheme 1) $^{[2-4,50-55]}$ this review will start by summarizing characterization techniques of electrolyte structures. $^{[24,28,56-58]}$ Then, the cationic coordination and

aggregation structures from Li-based dilute solutions (around 1 mol dm⁻³) to HCEs, then to LHCEs, will be summarized and their connections to cell performance will be understood. In the end, principles for efficient electrolyte screening and novel electrolyte design will be proposed based on these fundamental understandings between electrolyte aggregation structures and electrochemical properties. This review provides an in-depth understanding and assistance on the electrolyte screening and the development of new electrolyte systems.

2 | CHARACTERIZATIONS OF ELECTROLYTE STRUCTURES

2.1 | Raman spectroscopy

The vibrational spectrum provides frequencies, intensities, and band properties which have the ability to identify species and understand the related chemical processes. Till now, numerous works have applied vibrational spectroscopy to probe the interactions between salts and solvents in electrolytes. [28,59-62] Raman spectroscopy is one of the most frequently used techniques in electrolytic system, which was first adopted in poly(ethylene oxide) electrolytes, presenting the correlation between spectroscopic data and electrolyte viscosity and conductivity. [60] Then, it has been applied to monitor the solution structural evolution along with the concentration change in both organic and aqueous electrolytes.

The solvents of organic carbonate are largely applied in both academic and industrial areas, including PC, EC, dimethyl carbonate (DMC), and mixed solvent, coupled with proper lithium salts, performing its functionality in battery system. Raman technique has been widely applied to detect the solvation of lithium salts and the mechanism of ionic conduction, so that the factors which affect the performance of the carbonate-based electrolytes can be well identified. [28,62,63] As shown in Figure 1A, Kondo et al. [62] presented that the signal at 712 cm⁻¹ is assigned to the ring-deformation band of free PC. Along with the increasing of electrolyte concentration, the Raman band at 712 cm⁻¹ was separated into two components, 712 and 721 cm⁻¹. The new generated band derives from the interaction between PC molecule and Li⁺, which is also verified by Battisti et al. [60] The intensity increases as the LiPF₆ concentration increases,

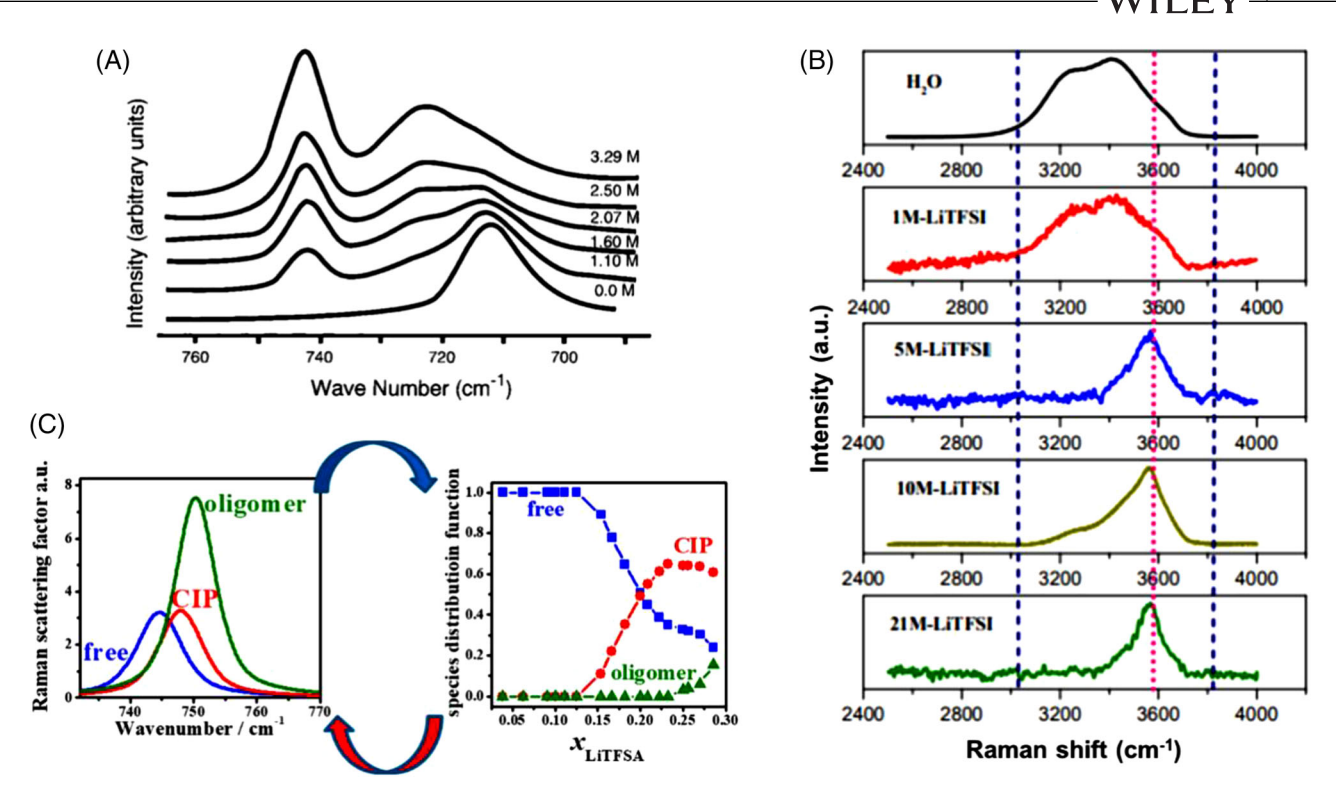


FIGURE 1 (A) Raman spectra of PC-LiPF₆ with various salt concentrations.^[62] (B) Raman spectra of aqueous electrolytes with different LiTFSI salt concentrations.^[24] (C) Raman scattering factors (left) and the corresponding species distribution functions (right) as the function of the molar fraction of LiTESA^[72]

corresponding to the decreased trend of solution viscosity and conductivity. Recently, Hwang et al. [28] gave a detailed demonstration about the ion speciation and related content of 0.1-3 M LiPF₆ and LiBF₄ in PC solvent. In LiPF₆-PC solution, there are two peaks at 741 and 746 cm⁻¹, both of which originate from the presence of PF₆⁻. The first peak is assigned to the free anions and solvent-shared ion pairs (SIPs), [64,65] and the second peak is attributed to contact ion pairs (CIPs) and contact dimers (CDs), respectively. [66,67] Notably, the solvent-shared dimers (SSDs), a dimer of SIP, are presented at the first peak for comparison although there is no evidence now. [66] However, the Raman spectrum obtained in LiBF₄-PC solution presents different peaks of Li salt compared to that in LiPF₆-PC solution. There are three peaks observed centered at 766, 773, and 783 cm⁻¹ in the LiBF₄-based electrolytes, corresponding to free anions and SIPs (first peak), CIPs, and CDs (second peak), and higherorder agglomerates (AGGs), respectively. [68] Coupled with dielectric relaxation spectroscopy (DRS), the quantitative information of the ionic speciation was acquired. Moreover, the variation trend as a function of electrolyte concentration was presented. The results showed that when the electrolyte concentration was controlled under 0.8 M, the free ions and SIPs are the dominant species, while only SIPs dominate when continuing to enhance the electrolyte concentration up to 0.8-1.5 M. However, as for higher concentration electrolytes (1.5-3 M), the dominants in LiPF₆-PC and LiBF₄-PC solutions are different, which are attributed to SSDs/CDs and CIPs/CDs/AGGs, respectively.

In aqueous-based electrolytes, Raman spectroscopy was also an efficient technique to determine the solution structure. [11,24,69,70] Suo et al. [11,71,72] investigated the interplay among Li⁺, TFSI⁻, and $\rm H_2O$ molecule by the Raman vibrational signals. As the salt concentration increases, the

Raman peak at 744 cm⁻¹ shifts to a large value (748 cm⁻¹ at 21 M) owing to the formation of TFSI⁻ anionic network, ^[73] proving the existence of solution aggregation phenomenon. Zheng et al.[24] presented a comprehensive study about the solution structure evolution from dilute to high concentration aqueous electrolytes by the application of both LiNO3 and LiTFSI. In pure water, H₂O molecular clusters are formed by hydrogen bonding and present a broad Raman band corresponding to the O_H—H stretching vibration.^[74,75] In high salt concentration solutions, a new peak at high wave number appears and the broad band of pure water disappears at the same time (Figure 1B), correlating to the increasing Li⁺-O_H interaction to replace hydrogen bond. Coupled with the complementary least-squares analysis (CLSA) during the Raman spectroscopic experiments, Hikari et al. quantitatively revealed the Li⁺ local structure in the LiTFSI aqueous solutions.^[71] The peak at around 744 cm⁻¹ is attributed to the S-N symmetric stretching vibration coupled with CF₃ bending of TFSI anion, which shifted to high wave number with elevated salt concentration. Moreover, the detailed solution structure evolution from dilute to concentrated electrolytes were presented in Figure 1C, in which the variation from free TFSI- to CIP TFSI-, and then to the bidentate TFSI⁻ and/or the oligomer TFSI⁻.^[72]

2.2 | Infrared spectroscopy (IR)

IR is another type of vibrational spectrum to define the intramolecular vibrations and the characteristic bonding of atoms. Moreover, the infrared signals are strong and can be calibrated for quantitative measurements using univariate and multivariate methods. This feature has extended its application in studying various electrolyte systems. [56,63,76–79] In

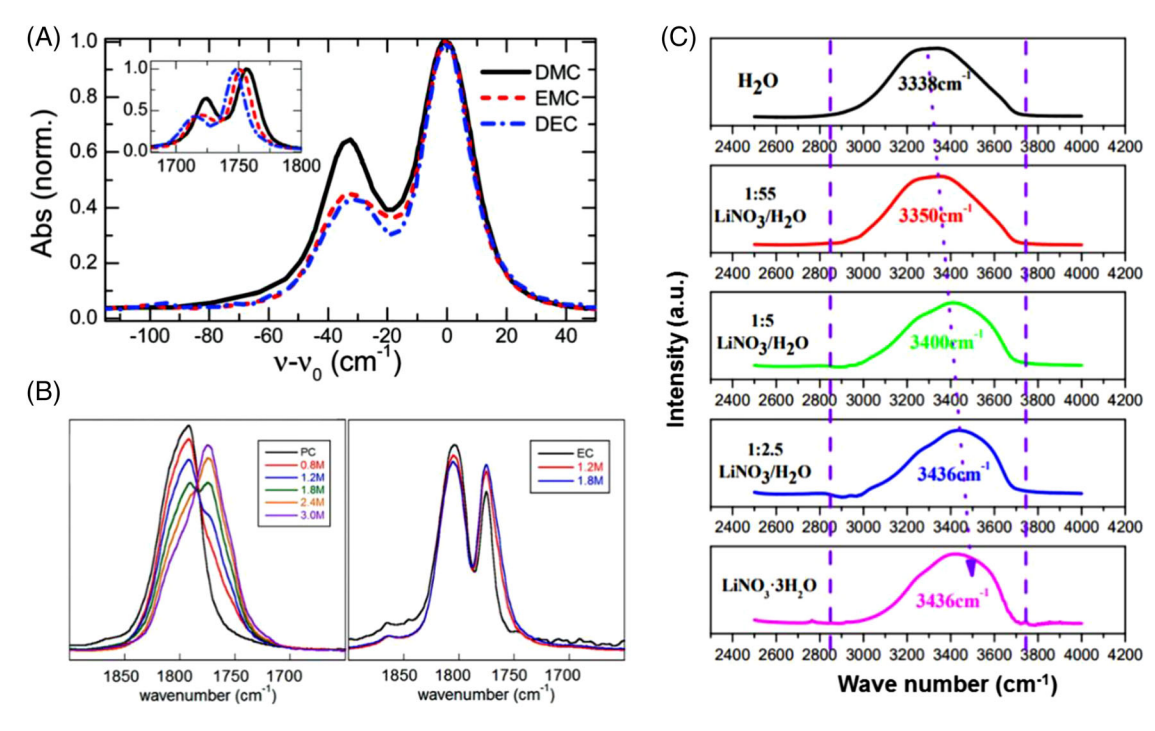


FIGURE 2 (A) Normalized and centralized FTIR spectra of LiPF₆ in DMC, EMC, and DEC at X(LiPF₆) = 0.09. The inset is the non-centralized spectra. [76] (B) FTIR spectra of carbonyl group in PC-based (Left) and EC-based (right) electrolytes with the variation of LiPF₆ concentration. [78] (C) Infrared spectroscopy of LiNO₃ solution with different concentrations^[24]

2000, Barthel et al.^[77] recorded the FTIR spectra of LiClO₄ in acetonitrile (AN), benzonitrile (BN), and PC, respectively, followed by spectra fitting and calculation, presenting the solvation number and solution structure components. Fulfer et al.^[76] compared the different solvation shell structure produced by linear organic carbonates (DMC, EMC, DEC) with different chain lengths by FTIR. As shown in inset of Figure 2A, where two peaks can be observed in linear IR spectra. The peak located at high frequency mainly corresponds to the free carbonyl peak donated as the free carbonyl stretch, while the low-frequency peak is assigned to asymmetric carbonyl stretch modes from the formed tetrahedral solvation shell of Li+ denoted as the coordinated carbonyl stretch.[77-79] According to the IR experiments, it is known that there are more coordinated bands in DMC solution and either linear carbonate forms a tetrahedral solvation shell (coordination number of 4) around Li⁺. [78–81] The predominant species in different carbonate-based organic electrolytes with different concentrations were studied by Daniel et al. [78] Relying on the strong IR absorption of C=O bond in carbonate functional group, the variation processes of IR spectra along with the change of salt concentrations were captured. As compared in Figure 2B, with PC solvent and high salt concentration condition, the coordination of PC to Li⁺ causes the uncoordinated PC at 1805 cm⁻¹ and Fermi resonance at 1790 cm⁻¹ shift to 1772 and 1750 cm⁻¹, respectively. However, in EC solution, owing to the C=O stretch band overlap between coordinated EC and Fermi resonance, it is hard to realize meaningful deconvolution.^[82,83] Based on the obtained C=O IR spectra in different solvents (PC, DMC, DEC), the solvent coordination number were presented and it decreases from dilute to concentrated electrolytes, which is attributed to the presence of ${\rm PF_6}^-$ anion in the coordinated sphere of Li⁺ compensating the reduced solvent molecules in high concentration condition. In aqueous electrolyte, the

infrared bands in the range of 2500-4000 cm⁻¹ correspond to the O-H stretching modes of water molecules, which was applied for the solution structure variation detection by Zheng et al.^[24] As shown in Figure 2C, the peaks centered at 3338 and 3350 cm⁻¹ are associated with the O_H-H stretching vibration in pure water and dilute LiNO3 solution, respectively. Along with the increase of electrolyte concentration, these peaks shift to high wave number and become sharper, indicating the gradually decreasing content of hydrogen bonds.

Nuclear magnetic resonance (NMR) 2.3

NMR utilizes a strong static magnetic field along with a weakly oscillating field surrounding the sample to induce and measure changes in the magnetic properties of the selected atomic nuclei, which was first regarded as an important technique to study the solution effects by Arnold and Packard in 1951.^[84] Along with the increase of electrolyte study, including aqueous and non-aqueous solutions, the structure information has been considerably advanced by the application of NMR.[24,85-89] Normally, natural abundance ¹⁷O and/or ⁶Li NMR spectra were employed to study the solvation structures of electrolytes, based on the changes in chemical shift and linewidth at ultrahigh magnetic field, while ¹³C spectrum can only provide indirect probe of Li+ solvation leading to the difficulty in information quantification. [86,87,90]

Xu et al. [86] conducted ¹⁷O NMR measurements to investigate traditional carbonate-based electrolytes. As shown in Figure 3A, with the addition of Li salt, the peaks of carbonyl ¹⁷O (a and c) experienced a low-value displacement due to the shielding effect of Li+ on the lone pair electron density, while the ethereal ¹⁷O (b and d) presented a high-value displacement owing to the increased deshielding

FIGURE 3 (A) ¹⁷O NMR spectra for pure EC and DMC, the mixture solvent of EC/DMC and the mixture solvent with 1.0 M LiPF₆, respectively. ^[86] (B) The ¹⁷O NMR spectra of the electrolytes at different concentrations (in the left panel) and the region of tetraethylene glycol dimethyl ether (TEGDME) peaks (in the right panel) for the 0.1 and 0.5 m electrolytes. [92] (C) The changes of Li⁺ solvation structures with increasing LiFSI salt concentration in DME-based electrolyte by explaining the ⁶Li and ¹⁷O NMR spectra of electrolyte with different concentrations^[87]

effect.^[91] Additional NMR measurements were carried out to record the chemical shifts of 1 M LiPF₆ in EC and DMC mixtures with different ratios, proving that Li⁺ strongly contacts with EC over DMC in traditional non-aqueous electrolytes. Moreover, after quantifying chemical shifts, the Li⁺solvation sheath was also revealed, in which the maximum of six EC molecules can coexist. Piercarlo et al. [92] carried out the NMR measurements with the combination of ¹⁷O and ⁶Li detection at their natural abundance, performing a deep investigation of the solvation structure of Li⁺ in the applied solution. As exhibited in Figure 3B, the NMR results proved that Li-ions are chiefly associated with the adopted anion and coordinated with one or two solvents in concentrated solutions, which helps better understanding of the main species in the formed SEI layer for good operation of Li metal batteries. Jianzhi et al.^[87] collected the natural abundance ¹⁷O and ⁶Li spectra of LiTFSI in dimethoxyethane (DME), coupled with quantum chemistry and molecular dynamics (MD) studies, demonstrating the evolution of solvation structure of Li⁺ with enhanced salt concentrations. As presented in Figure 3C, which helps obtain comprehensive understanding of the electrolyte structure and its effects on the performance of electrolytes.

Small angle X-ray scattering (SAXS)

SAXS is a non-destructive method for electrolyte nanostructure characterization. Moreover, its excellent time-resolution enables capturing the MD during operando test. SAXS was first applied for the research of Al-Cu alloy by Guinier and the related results were published in 1938.^[93] Owing to its widely used features, SAXS method experienced tremen-

dous development and extension, initially from polymerbased systems to material science. Nowadays, it was applied for studying electrolyte structure, which is an ideal complement to other methods, such as Raman, IR, and NMR. In 2021, Li et al. did a comprehensive review focusing on the microscopic understanding of liquid electrolytes by SAXS and operando SAXS. Moreover, the theory of SAXS method, SAXS data collection, processing, and analysis were also discussed for better understanding.^[58]

Figure 4A presents the optical components of the 12ID-B SAXS beamline at the Advanced Photon Source. The scattering vector q is the distance between two positions and applied for data analysis. Hence, based on the perspective of the distance distribution in the applied liquid electrolytes, we can obtain the detailed solution structure information. For the high-q part $(q > 0.6 \text{ Å}^{-1})$, it can be attributed to the size and shape of molecules or clusters; the middle-q part (0.6 Å⁻¹ > q > 0.05 Å⁻¹) is decided by the spacing change between molecules; the low-q part $(q < 0.05 \text{ Å}^{-1})$ presents the large particles or aggregation (diameter > 12.5 nm) in the electrolytes.^[58] Based on this information, the solution microstructure was identified accordingly. [94-97] Feng et al. [94] studied the microstructures of the widely applied LiPF₆/carbonates electrolytes by SAXS, in which the selected solvents are EC, PC, EMC, and DEC. It was found that there are small clusters in the mixture of EC and linear carbonate and the mean diameter of the nano structure is around 1 nm (Figure 4B,C). Aguilera et al.^[95] did a comprehensive study about the solution structure of LiTFSI-tetraglyme (G4) mixtures from dilute solutions to concentrated solutions by SAXS (Figure 4D), where a board peak can be observed at 1.5 $Å^{-1}$, which is attributed to the intermolecular distances. The formed new peak at high

FIGURE 4 (A) Small-angle X-ray diffraction setup at the Advanced Photon Source (APS). The above inset describes the difference between small and wide angle X-ray scattering.^[58] (B,C) SAXS data of EMC, EC/EMC, DEC, and EC/DEC.^[94] (D) SAXS data of the solutions comprising of LiTFSI and tetraglyme with different ratios^[95]

concentration condition is considered as the distance between Li⁺/G4 and TFSI anions, or the entirety of the two parts. Moreover, the SAXS technique has been employed in the study of aqueous electrolytes, and lots of groups have monitored the existence of heterogeneous domains in high concentration solutions (water-in-salt electrolytes). [97,98] According to the above conclusion, it is known that SAXS has the ability to provide global view of the solution structures, including clusters, aggregates, and nano-domains.

2.5 | Molecular dynamics (MD)

Classical force-field-based MD simulation is a powerful tool for providing an in-depth understanding of the structure and kinetics of solution systems. It enables investigation of systems with up to thousands of atoms on the scale of microseconds. Nowadays, the parametrization in force fields for molecular solution systems has been achieved, which are reliable within a wide temperature range and a variety of molecules. [99] In early studies, nonpolar systems were modeled using traditional nonpolarized force fields, but they could hardly deal with polar systems, with the predicted thermodynamic and kinetic properties significantly different from the experimental results.^[100-102] Recent studies tried to establish the polarized force fields,^[103] such as the fluctuating charge model, [104] classical Drude oscillator model, [105] and induced point dipoles.^[106] With these models in classical MD simulations, it is feasible to inspect the physical and chemical processes for lithium salts in a solution, including the solvation and transportation of ions.

There are numerous works focused on classical MD simulations of lithium salts in solutions. For example, Wang et al. used MD simulations to study the Li⁺ transport behav-

ior in poly(ionic liquid)-in-salt electrolytes, demonstrating the unusual co-coordination of the anion between the polymer backbone and the Li+.[107] Two Li+ sharing connected FSI- coordination was shown to hop in a correlated manner, which is analogous to the phenomenon in high salt concentration ionic liquid systems.[108] Amanchukwu et al. synthesized a group of ionically conducting fluorinated ether electrolytes and utilized classical MD simulations to facilitate the microscopic understanding.^[109] They showed that the fluorinated ether coordinates with Li⁺ while the fluorinated segment coordinates preferentially with the FSA-, indicating that long ether segment and short fluorination are beneficial to the ionic conductivity. As shown in Figure 5A–D, Wang et al. used DFT-MD simulation to help study the evolution of solvated structure from diluted to concentrated electrolyte.[110] Figure 5B shows the simulated structure of diluted solution, where almost all the DMC solvents are in a free state since there is high solvent-to-salt molar ratio. As the increase of Li salt concentration, the simulated structure of moderately concentrated solution in Figure 5C displays that almost 90% of DMC solvents participate in becoming a part of a common four- or fivefold coordinated state with Li⁺ and all the anions of Li salt coordinates with Li⁺ by the forms of about 20% as CIPs and about 80% as AGGs. For the concentrated solution, the simulated structure exhibited in Figure 5D reveals that there are no free solvent molecules and salt anions observed except coordinated with Li⁺. Moreover, the anions remain in AGG states where nitrogen on salt anions are found to coordinate with Li⁺ besides oxygen, resulting in a reinforced 3D network. This unusual solution structural feature in concentrated solution is responsible to suppress the transition metal ions dissolution from highvoltage cathode due to lower probability of coordination with free solvents and anions, and simultaneously decrease their



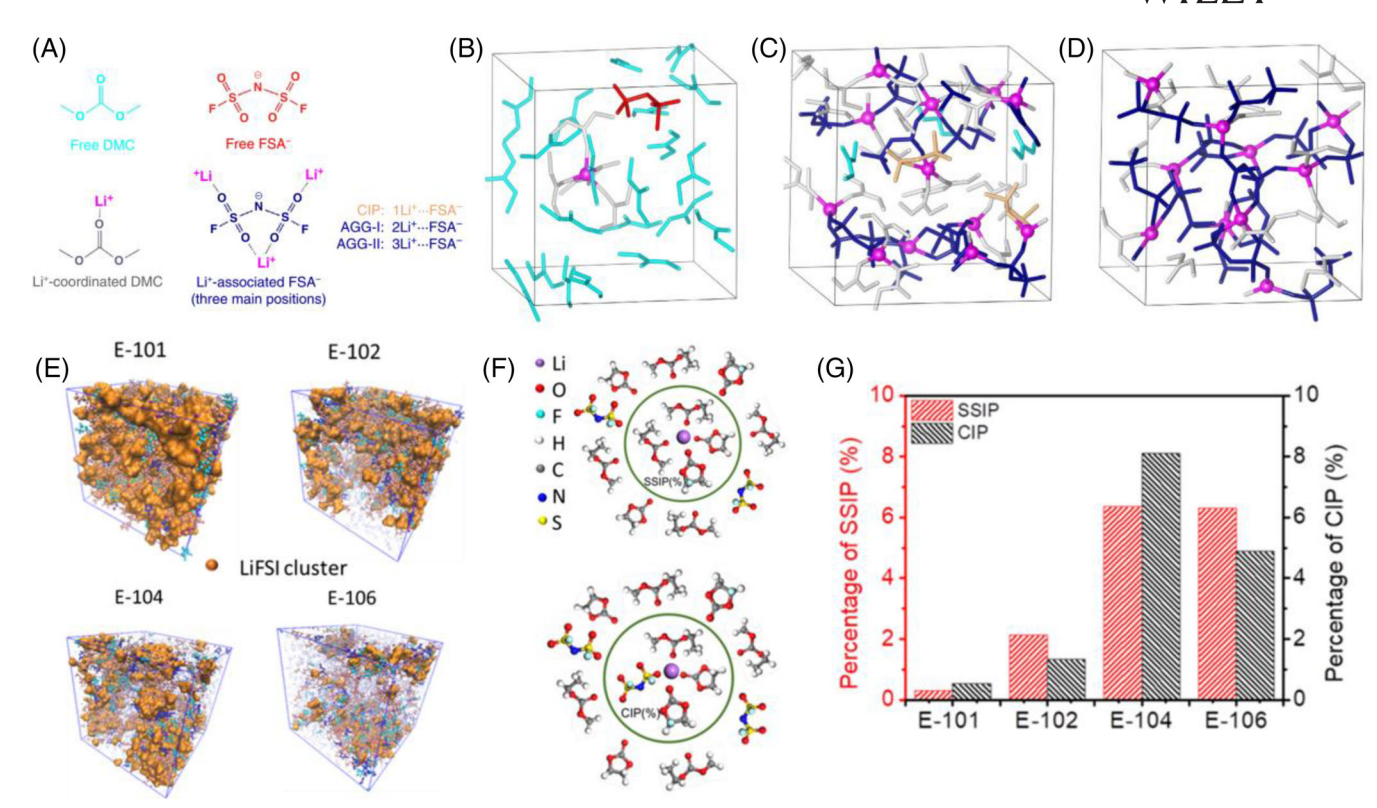


FIGURE 5 (A-D) DFT-MD simulations to understand evolution of solvated structure from diluted to superconcentrated electrolyte. (A) The illustration of main species and their coordination structure in the LiFSA/DMC solutions. (B-D) Typical equilibrium trajectories snapshot from DFT-MD simulations based on electrolytes with different salt concentrations: (B) diluted solution (less than 1 mol L^{-1}), (C) moderately concentrated solution (about 4 mol L^{-1}), and (D) superconcentrated solution (about 5.5 mol L⁻¹).^[110] (E–G) MD simulations to understand the effects of the addition amounts of BTFE diluent on solution structure of LHCE. (E) MD snapshots of different LHCEs at 303 K. (F) Illustrations of different Li+ clusters of SSIP and CIP dependent on the first solvation shell of Li⁺. (G) Percentage change of SSIPs and CIPs with increasing molar ratio of fluorinated diluents to carbonate solvents from E-101 to E-106[111]

subsequent diffusion rate, finally leading to a high-voltage LiNi_{0.5}Mn_{1.5}O₄/graphite battery with excellent cycling durability. MD simulation can also be performed to study the coordination structure and ionic diffusion kinetics based on LHCE. As shown in Figure 5E–G, Jia et al. prepared a series of LHCEs with different contents of BTFE as fluorinated diluents added and investigated the effects of BTFE on solution structure, resulting in different electrochemical performance when used in Si-based LIBs.[111] Figure 5E shows MD snapshots of different electrolytes using LiFSI as salt with increasing molar ratio of fluorinated diluents to carbonate solvents from E-101 to E-106. As the proportion of BTFE increases, the percentage of small LiFSI-EC/EMC-FEC clusters enhances. There exist two kinds of solvated structures of SSIP and CIP in the LHCE, dependent on the first solvation shell of Li⁺ as depicted in Figure 5F, the proportion of which does not strictly linearly relevant with the amount of BTFE added. As listed in Figure 5G, there remains highest proportion of SSIPs and CIPs and the fastest ionic diffusion in the LHCE of E-104, which almost cannot be easily detected in the electrolyte of E-101 without BTFE added, where most of Li⁺ form clusters with salt anions. This optimized and unique solution structure regulated by appropriate diluent is conducive to form a stable interface between electrode and electrolyte with excellent ionic diffusion kinetics, hence improving the performance of electrode.

In addition to the above frequently applied methods for electrolyte structure detection, some other techniques such as X-ray pair distribution function (PDF) and neutron diffraction were also used cooperatively. PDF technique has gained

expanding impact on material region for quantitating material structure information under the limitation that the structural coherence shows in a few nanometers.[112] For electrolyte structure study, it was adopted to quantitate the bond-length between different atoms to show the inner structure, but it is not easy to play an effective role in complex electrolyte system.^[24] Neutron diffraction with isotopic substitution can detect the coordination structure around the isotopically substituted element, which was also widely applied.[113] However, for better and accurate understanding of the liquid solution structure, combination of characterization techniques is recommended, such as the NMR test/quantum chemistry/MD, [87,114] Raman/FTIR/PDF/MD, [24] and FTIR/ NMR/DFT simulation^[78]. These fundamental structural understandings are helpful for recognizing the macroscopic physical properties of the applied electrolytes, and understanding overall electrochemical performance, such as cycle ability, rate performance, high- and low-temperature performance, and safety.

LI-BASED DILUTE ELECTROLYTES 3

Traditional dilute electrolyte structure 3.1

In aqueous electrolyte, the hydration structure of Li⁺ has been experimentally and theoretically studied in the past decades. [57,115-117] In general, every four water molecules existed in the primary solvation sheath are coordinated to one Li⁺ center to form a cationic aggregation of Li⁺(H₂O)₄ as

Schematic illustration of Li⁺ solvation sheath in both dilute aqueous and organic electrolytes. (A) In dilute aqueous electrolytes, there are four water molecules in the primary solvation sheath coordinated to each Li⁺ center forming a cationic aggregation of Li⁺(H₂O)₄. [11] (B) In dilute organic electrolytes, such as EC-containing mixture, a complex cationic aggregation of Li⁺(EC)₄ is formed in the primary solvation sheath^[86]

depicted in Figure 6A. In 1995, Rudolph et al. collected the Raman spectra from LiCl saturation concentrations to more dilute solutions at room temperature, where the new band at 255 cm⁻¹ corresponds to the Li–O symmetric stretching of Li(OH₂)₄+.[115] Loeffler et al. studied the Li⁺ hydration structure via combined simulations, which suggest dominant fourfold coordination of Li+ with small amounts of fivefold coordination structure observed.[117] Moreover, the average distance of Li-O bonding in Li(OH2)4+ was obtained for better understanding of the solution structure. As for the four-coordinated Li⁺ in aqueous solution, the corresponding distance of Li-O bonding is 1.942 Å.[57] Compared to other alkali metal ions, the size of Li+ is smaller, so it has a stronger tendency for hydration. Hence, theoretical simulation suggests that a second hydration shell is very likely to exist in the Li⁺ hydration structure, which can be denoted as $[\text{Li}(\text{H}_2\text{O})_4^+](\text{H}_2\text{O})_n (n = 4, 8).$ ^[116]

In organic electrolyte, there is almost the same coordination structure as presented in aqueous electrolyte. To explore the local structures of Li⁺ in mixed organic solvent-based electrolyte, ab initio molecular orbital calculations were carried out to figure out the Li⁺ coordination structure and it was found that compared with methylethyl carbonate (MEC), Li+ was preferentially coordinated to EC with a coordination number of 4.[118] Xu et al. conducted ¹⁷O NMR study to determine the interaction modes of Li⁺ with carbonate molecules, to quantitatively analyze the Li⁺-solvation structure in different solvents. The results also showed that Li⁺ was preferentially coordinated with EC molecules than DMC. The strong bonding tendency between Li+ and EC can be explained by the large solvation energy due to the existence of carbonyl. Despite the weak bonding between Li⁺ and DMC, DMC can be still found in the Li⁺ solvation sheath. These findings have drawn a clear picture of Li⁺ solvation structure for the first time (Figure 6B).[86]

3.2 | Electrochemical performance of dilute electrolyte

Generally speaking, the ionic conductivity of an electrolyte increases with salt concentration when it is below 1 mol dm⁻³ (1 M). However, with a further increase of salt concentration, it experiences a monotonic decrease (Figure 7A).[119]

Therefore, 1 M has been regarded as the optimal electrolyte concentration and widely adopted. Therefore, it is of significance to give a detailed analysis about their solution structure and associated electrochemical behaviors of Li⁺ to establish the correlation between solution structure and electrochemical performance. Table 1 shows the development and influence of dilute electrolyte categories on battery performance.

As mentioned above, there are four solvents coordinated with each Li⁺ in both aqueous and aprotic electrolytes, hence desolvation processes must take place before Li⁺ diffuses into the applied electrode materials. Understanding how Li⁺ diffuses in bulk electrolyte and their desolvation on interface are critical to estimate the energy barriers related to the electrochemical performance, especially for rate capability. Zheng et al. presented a detailed Li⁺ diffusion process both in water-based and EC-based organic electrolytes as shown in Figure 7B,C,[127] where LiFePO₄ was chosen as electrode material for study, owing to its stable and simple olivine crystal structure providing one-dimension Li⁺ diffusion channel. As illustrated in Figure 7D, in aqueous system, two water molecules need to be stripped away from the cationic aggregation of Li(OH₂)₄⁺ and then reach the formed Janus interface, where the truncated symmetry of solid LiFePO₄ surface is compensated by the chemical absorption of H₂O molecules, resulting in a complete interface with a half-solid (LiFePO₄) and a half-liquid (H₂O). After Li(OH₂)₂⁺ arrives to the Janus interface, Li⁺ diffuses into the bulk of electrode material along the Li⁺ channel while the coordinated H₂O two water molecules will be desorbed and dock at the surface to compensate for the broken symmetry ((iv) in Figure 7B). By comparing energy barriers at different stages, including Li⁺ diffusion in bulk electrolyte, Li⁺ desolvation at the interface, and Li+ migration in the bulk of electrode material, it was found that the major kinetic hindrance derived from the desolvation process of Li⁺. However, the desolvation process in EC-based electrolyte is different compared to that in aqueous as illustrated in Figure 7C: (1) only one EC molecule is adsorbed on the solid electrolyte interface owing to the steric hindrance; (2) three EC molecules need to be stripped to finish desolvation when approaching the interface; (3) because of the poorly formed interface where just one EC is absorbed, Li⁺ must overcome a higher barrier to cross this interface. The well-formed Janus interface in water-based electrolyte contributes to its better electrochemical performance than the

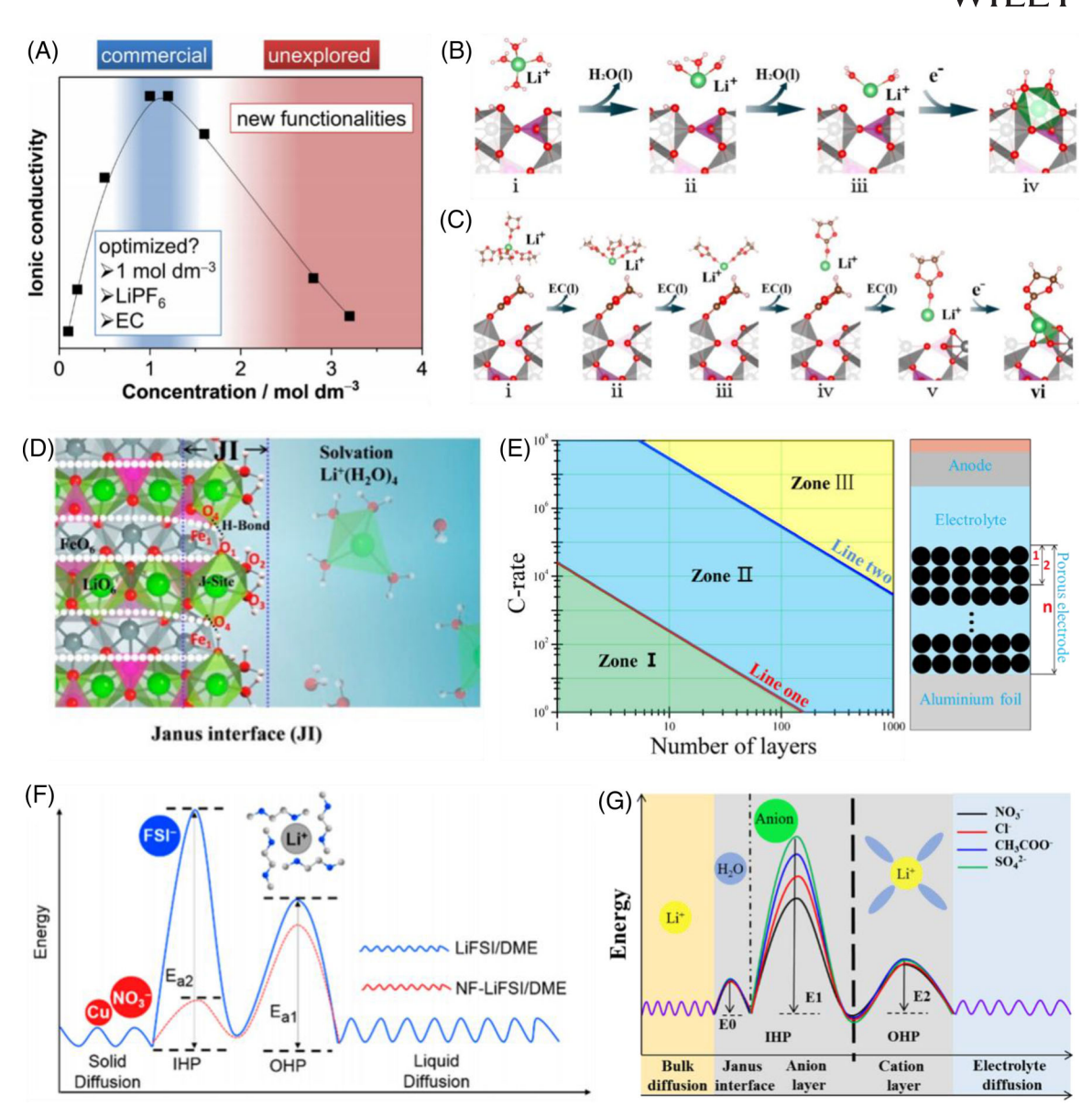


FIGURE 7 (A) The effects of salt concentration in electrolyte on its ionic conductivity, where the salt and solvent selected are LiPF₆ and EC, respectively.^[119] (B,C) Illustration of Li⁺ transport process across the FePO₄/water interface (B) and FePO₄/EC interface (C) during discharge. [127] (D) Schematic diagram of the formed Janus interface between LiFePO₄ cathode and aqueous electrolyte. [127] (E) The dominant factors that limit Li diffusion under different C-rate and electrode layers obtained by Pseudo Two-Dimensional Hidden Markov Model (P2D-HMM). [128] (F) The relationship of energy barriers of Li⁺ migration in the IHP and outer Helmholtz plane (OHP), which are denoted as E_{a1} and E_{a2} , respectively. [55] (G) The effects of specific adsorption in IHP and OHP on the energy barriers of Li⁺ diffusion, which are denoted as E1 and E2, respectively [129]

TABLE 1 Battery performance of low concentration electrolytes in representative studies

Electrolyte	Cathode/anode	Operation window	Capacity retention	Ref.
1 M LiAsF ₆ /PC-EC	Graphite/Li	0.02-1.2 V	>95% after 99 cycles	[120]
1 M LiBF ₄ –LiBOB/PC-EC-EMC	LiFePO ₄ /Li	2.0-4.2 V	Operate from -40 to 80°C	[121]
1 M LiPF ₆ /EC-PC-EMC+2%FEC	LiFePO ₄ /Li	2.5-4.2 V	97.5% after 300 cycles	[122]
1 M LiPF ₆ /EC-EMC+1%LiPO ₂ F ₂	NMC532/Graphite	3.0-4.3 V	96% after 3500 cycles	[123]
1 M LiPF ₆ /EC-EMC+2%VC	NMC70/Graphite	2.6-4.3 V	83.7% after 500 cycles	[124]
1.5 M LiPF ₆ /EC-EMC-DMC+1%LiPO ₂ F ₂	NMC811/Graphite	2.6-4.2 V	80% after 1000 cycles	[125]
1 M LiPF ₆ /EC-EMC+0.2%ATCN (5-acetylthiophene-2-carbonitrile)	LiCoO ₂ /Li	3.0-4.5 V	91% after 200 cycles	[126]

aprotic one, achieving excellent rate performance. Owing to high ionic conductivity in dilute electrolyte, it has been considered not to be the rate-determining step on Li⁺ diffusion, so its connection with rate capability of cells is rarely studied. However, when the applied C-rate is very high in a very

thin electrode, the ability of Li+ diffusion in the bulk of electrolyte should be reconsidered. As explained in Figure 7E, the inserted red and blue lines present the diffusion coefficients. In Zone I, the speed of Li⁺ diffusion mainly depends on its motion inside the active materials; In Zone II, Li+

diffusion relies on the combined action between the bulk and the electrolyte; while in Zone III, the electrolyte and the porosity of electrode would play a dominating role in the overall Li⁺ diffusion.^[128]

The choice of Li salt and solvent is also important for dilute electrolytes, as compared in the last paragraph demonstrating that water-based electrolyte is good for interface dynamics than EC-based electrolyte, which presents different solution structures and interface absorption properties resulting in variable electrochemical performance. Combining with the understanding of Li⁺ behavior in the bulk of electrolyte, Hu et al. studied the effects of applied Li salts on the interface dynamics. [55] As exhibited in Figure 7F, with the same cation layer and Janus interface, the anion layer in inner Helmholtz plane (IHP) has a significant influence on the Li⁺ diffusion process cross interface, where Li salt molecules with a smaller anion and higher dissociation degree present fast interfacial electrochemical kinetics. In organic electrolyte, Chong et al. studied the effects of adsorption layer on the formation of SEI layer by introducing functional ions, leading to excellent electrochemical performance such as an high average Coulombic efficiency of 99.5% over 500 cycles. [129] As shown in Figure 7G, Hailemariam et al. researched the species adsorbed on the surface of Li anode using density functional theory (DFT), and proved that Li⁺(EC)₄ cluster was more stable than Li⁺ aggregation comprising of both EC and fluoroethylene carbonate (FEC) solvents. However, the absorption energy of Li⁺(EC)₄ cluster on Li anode was weaker, which was bad for the formation of a strong SEI. Moreover, the authors also demonstrated that the anion-rich adsorbed species were conducive to a better SEI to stabilize Li anode. The structure of a mixed carbonate/LiPF₆ solution as a function of electrode potential was investigated by MD. It was found that the increasing amount of EC on the interface of both positively and negatively charged electrodes is responsible for high-quality SEI layer. [4,49,130] With increasing electrode potential, the density of PF₆⁻ increases rapidly.^[49]

Based on the above discussion, it is clear that there are abundant free solvents in dilute electrolytes and each Li⁺ tends to be coordinated with four solvents. When factors come to the influence on battery performance, the desolvation process inside the electrolyte should be primarily considered since it has to do with Li⁺ dynamics resulting in different electrochemical performance. In addition, electrode–electrolyte interface plays a vital role on cell performance, including cycling stability, interfacial kinetics, and coulombic efficiency, which depends on the applied solvent and salt. Therefore, the category of salt and solvent and the ratio between the applied solvents should be carefully chosen as they are closely related to battery performance.

4 | CONCENTRATED LI-BASED ELECTROLYTES

4.1 | Structures of HCE and LHCE

To further improve the energy density of Li batteries satisfying the ever-increasing marketing requirements, the most promising strategy is to expand the operating voltage window.^[131,132] However, due to their intrinsic thermody-

namic instability under extreme potentials, commonly used dilute electrolytes are still insufficient to suppress excessive redox decomposition of the self and maintain the interfacial integrity to stabilize the structural changes on both cathodes and anodes during cycling, even causing safety concerns due to their flammability, finally seriously hindering the practical application of next-generation LIBs. [43] Therefore, different approaches especially replacing with highly safe solid electrolytes have been extensively attempted. However, there is still a long way to go until solving their well-known drawbacks of low ionic conductivity and weak compatibility towards electrodes along with unavoidable high interfacial resistance. [133] This even causes the upper current density for dendrite-free Li metal anode far below that in liquid electrolytes. As a compromised alternative, HCEs have been proposed and expected to satisfy commercial uses due to a series of outstanding properties including improved oxidation and reduction stability leading to wider electrochemical stability window for high-voltage LIBs, fast electrode reaction, reduced solvent volatility resulting in enhanced thermal stability and suppressed corrosion of Al current collector and dissolution of transition metal ions, especially for improved lithium plating/stripping performance avoiding wanton growth of lithium dendrites and suppressed representative shuttle effect in Li-S batteries.[31,44,134-136] To trace the root, it was found that when the concentration of Li⁺ in the electrolyte increases up to a certain point, the physicochemical properties of the solution phase and the associated interface phase will undergo drastic changes, thus leading to much of solvents and Li salts expected to be revitalized, which were previously thought to be incompatible with more aggressive anodes and cathodes. These changes were further found to be derived from solvation sheath reorganization of Li⁺.[137] In detail, as discussed above, most solvent molecules and Li salts are free in the dilute electrolyte, where nucleophilic solvent molecules tend to coordinate with Li+, simultaneously weakening the association between Li⁺ and anions, so that lithium salts are dissociated in the electrolyte. With the increase of Li salt concentration, the coordination competition between solvent molecule, anions, and Li⁺ determines the reorganized solution chemistry structure of the electrolyte leading to their respectively changed thermodynamic and dynamic stability, which finally changes the interfacial chemistry and improves the compatibility towards chemically reactive cathode and anode. As a result, the batteries using HCEs would show dramatically improved electrochemical performances, especially when operated at extreme conditions. As displayed in Figure 8A-E, Zheng et al. predicted local structure evolution of LiNO3 aqueous solution from diluted to highly concentrated LiNO3 aqueous solution by simulations, which also been validated by the atomic PDF analysis of high-energy X-ray and neutron diffraction.^[24] Results showed that a local structure originating from a condensed Li⁺-hydration sheath caused by intimate Li⁺-water interaction in the solution arises with the increasing concentration of LiNO₃ salt, then further constructing (Li⁺(H₂O)₂)_n polymerlike chains (a type of cationic aggregation) to replace the ubiquitous hydrogen bonding, where the distance between water molecules remains only 3.1 Å. The special inorganic polymer structure directly dictates the different thermodynamic and kinetic states of water molecules and salt anions, thus expanding the aqueous stability window to 2.55 V.

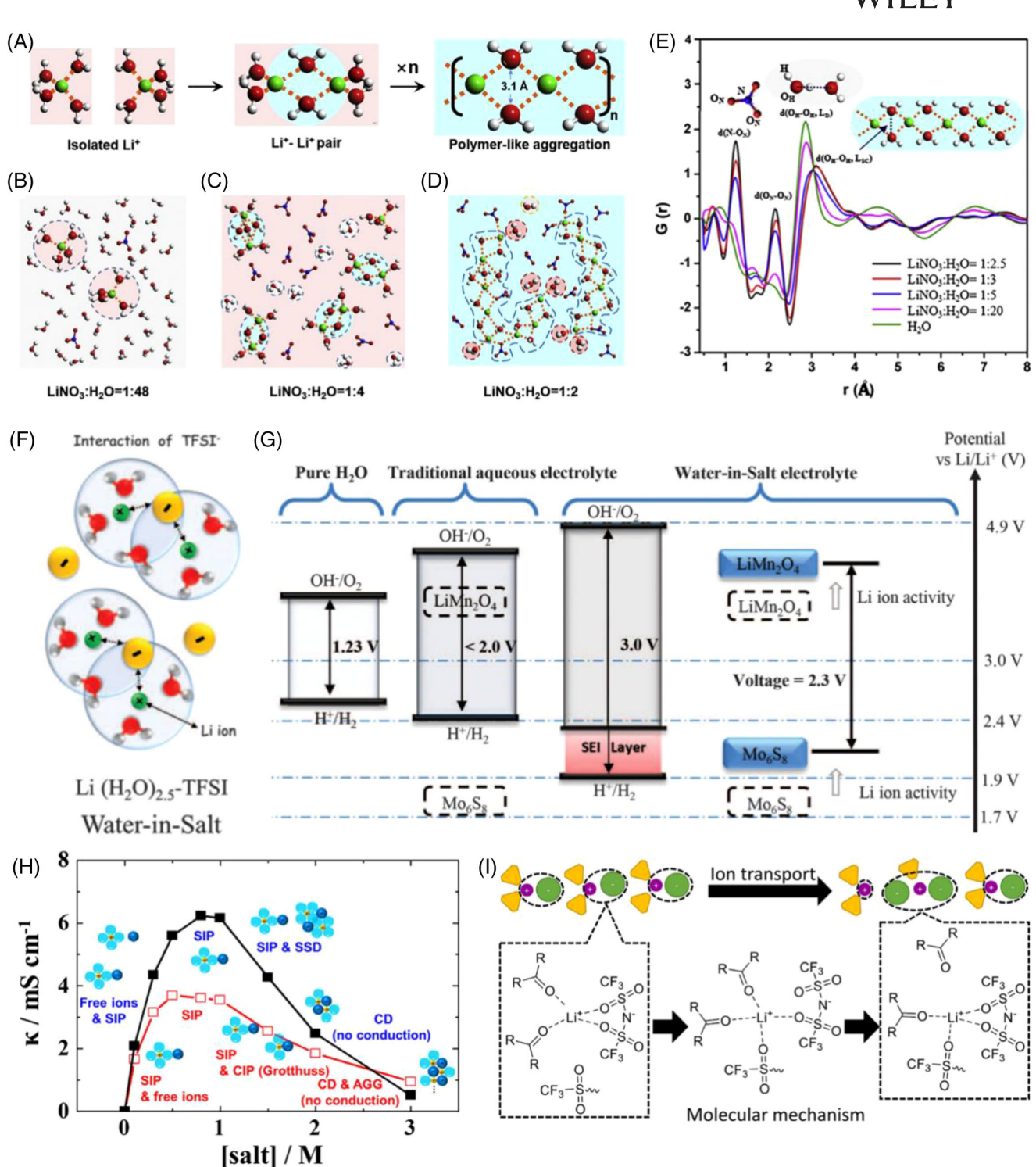


FIGURE 8 (A–E) Structural evolution of the LiNO₃ aqueous solution along with the increasing concentration by theoretical MD simulations (A–D) and experimental atomic PDF analysis of high-energy X-ray diffraction (E). [24] (F,G) Illustration of the structure of Li⁺ primary solvation sheath based on highly concentrated LiTFSI aqueous electrolyte (F) and comparisons of electrochemical stability window in different electrolyte systems. As for water-in-salt electrolytes with high salt concentration, their expanded electrochemical stability window enables the full Li-ion battery with the redox couples of LiMn₂O₄ and Mo₆S₈. (G). [11] (H) Summary of possible ionic species in LiPF₆-PC (black line with solid square) and LiBF₄-PC (red line with hollow square) electrolyte, respectively, with increasing salt concentrations and their corresponding ionic conductivity. [28] (I) Illustration of the exchange process of coordination and decoordination of solvent molecules from Li centers directly correlated to the breaking and bonding of interactions between the Li⁺ and the anion with increasing concentration of LiTFSI [56]

Suo et al. reported a highly concentrated LiTFSI aqueous electrolyte with an expanded electrochemical stability window of about 3.0 V by reconstructing the Li⁺ solvation sheath with more anions attached compared to the diluted solutions as predicted by MD simulation shown in Figure 8F, leading to the formation of a more stable electrode-electrolyte interphase as indicated in Figure 8G, which depends on an

interfacial chemistry dominated by the reduction of TFSI⁻ at interfaces instead of solvent molecules. ^[11] By using such a highly concentrated LiTFSI aqueous electrolyte, a full cell of 2.3 V prepared by coupling LiMn₂O₄ with Mo₆S₈ was enabled to cycle for more than 1000 times with improved rate capability. To fully understand the correlation of ion transport behavior and bulk structure of the electrolytes,

Hwang et al. examined the ionic speciation and conduction behavior of LiPF₆ and LiBF₄-based PC electrolytes respectively from dilute to high salt concentrations by combined complementary spectroscopic characterizations.^[28] As concluded in Figure 8H, different types and concentrations of Li salt have a significant effect on the interaction of ion-ion and ion-solvent finally leading to different aggregations, which dictate the main modes of ion migration in the specific electrolyte, hence the various ionic conductivity. Kankanamge et al. investigated the interactions and motions involved in LiTFSI-carbonvl electrolytes with different concentrations.^[56] As shown in Figure 8I, the process of coordination and decoordination between solvent molecules and Li centers, which is governed by the chemical nature of the solvent molecules, is directly affected by the interactions between the anion and the cation, leading to the small changes of solvent-solvent interaction potential, then resulting in totally different macroscopic properties of the electrolytes, such as its viscosity, hence the different ionic conductivity. Therefore, to enable high-performance LIBs, rational design of solution microstructure is a critical approach, which can be easily realized by HCE.

In addition to electrolyte viscosity, it is also widely accepted that the ionic conductivity of an electrolyte depends on Li⁺ concentration and mobility. Caused by close-knit 3D network of the solution structure based on HCE, the viscosity of the electrolyte increases and the movement of all the species in the electrolyte slows down, leading to its poor wettability and low ionic conductivity. These vital drawbacks have serious side effects on low-temperature cyclic performance and rate capability of Li batteries using HCEs. In addition, large amount of Li salts involved in the HCEs raises the cost question substantially because Li salts are more expensive than solvents. Therefore, there are still huge challenges ahead in the large-scale commercial application of HCEs. Recently, the so-called LHCE was put forward as depicted in Figure 9A, which refers to the addition of an inert diluent that is miscible with the solvent for avoiding solution phase separation but disable to dissolve the salt in HCE.^[35] As shown in Figure 9B, after the diluent is added, although the solution structure of the reinforced 3D network is broken, it does not affect the special solvation sheath of Li⁺ coordinated with the salt and solvent in the original HCE, thus forming the localized high concentration state of Li salt despite the decreasing content of Li salts per unit volume of electrolyte, which significantly reduce the cost of Li salts.^[138] This not only retains the merits originating from the solvation sheath of Li⁺ in the HCE, but also changes the undesired physicochemical properties to its own unique characteristics. For example, different Li⁺ transport mechanisms will lead to different ionic conductivity. Besides, its viscosity is much lower than that of HCE so that it has excellent wettability for both electrode and separator, resulting in effective usage of active electrode materials and improved rate performance. Therefore, diluents used for LHCEs need to meet the characteristics such as low dielectric constant, low complexation capacity, low viscosity, high wettability, low cost, non-flammability, and conducive tendency to form better interfaces. Currently, the most widely used fluoroether diluents and alkane diluents usually have the characteristics of low polarity, low dielectric constant, and low viscosity, and cannot dissolve Li salts.[139] Among, fluoroethers, such

as hydrofluoroether (HFE), 1,1,2,2-tetrafluoroethyl-2,2,3,3tetrafluoropropyl ether (TTE), and bis(2,2,2-trifluoroethyl) ether (BTFE), have high oxidation stability due to the electron-withdrawing fluorine atom and are considered as the most promising diluents for HCEs. [33,140] In summary, LHCE seems to be the most promising electrolyte for realizing a better Li battery with high-energy-density and high-powerdensity.

4.2 **Battery application of concentrated electrolytes**

Apart from the different physical and electrochemical properties compared to dilute electrolytes, the performance in practical battery systems of HCEs and LHCEs is equally important. In this chapter, we will briefly summarize the battery performance of both HCEs and LHCEs in various types of lithium batteries (see detailed comparison listed in Table 2).

Aqueous rechargeable lithium batteries 4.2.1

Rechargeable aqueous LIBs are attractive for deployments in future due to their advantages in terms of safety, environmental friendliness, manufacture feasibility and cost over their non-aqueous counterparts. However, low-energydensity caused by the narrow electrochemical stability window of water (only 1.23 V), that is incompatible with most of cathodes developed in non-aqueous lithium batteries such as LiFePO₄, LiCoO₂, and LiMn₂O₄, severely hinders their commercial progress.[141] For better rechargeability, redox reactions of both electrodes must take place within the stability window of the matching electrolyte, which is dependent on the reductive and oxidative reactions of compositions involved. Therefore, optimizing the compositions of electrolyte to tune the structure and composition of the Li⁺ solvation sheath would influence thermodynamic and kinetic behaviors of original solvents and salts, leading to their expanded voltage stability window to improve the compatibility towards more prevailing electrode materials, then drastically improving the energy density of aqueous LIBs. Recently, a highly concentrated aqueous electrolyte, dubbed water-in-salt, is considered as the most promising and easy way to realize the commercialization of rechargeable aqueous LIBs. [11,142] Hu et al. clarified the effects of electrolyte concentration on Li⁺ thermodynamic and kinetic behaviors in aqueous electrolytes using LiFePO₄ as the active electrode by carrying out cyclic voltammetry and voltage profiles based on a customized single-particle model.^[54] As summarized in Figure 10A, the positive shift in the equilibrium potential with the increase of electrolyte concentration confirms the thermodynamic effect induced by the formation of $(Li^+(H_2O)_2)_n$ polymeric structure in concentrated aqueous electrolyte, which is beneficial for accurate determination of the working voltage range considering the balance between the delivery of cathode capacity and the electrochemical stability of the electrolyte. As illustrated in Figure 10B, various factors have significant impacts on the Li⁺ kinetic process. The polymeric structure formed by cation aggregation in concentrated electrolyte leads to a higher Li⁺ desolvation energy and lower interface reaction constants, thus slowing down Li⁺ diffusion through the

FIGURE 9 (A) Electrolyte structures of HCE and LHCE. [35] (B) Illustration of the change of the solution structure in HCE after adding different contents of diluent to form LHCE [138]

TABLE 2 Battery performance of concentrated electrolytes in representative studies

Electrolyte	Cathode/anode	Operation window	Capacity retention	Ref.
LiFSA/DMC (molar ratio of 1:1.1)	$ \begin{array}{l} LiNi_{0.5}Mn_{0.5}O_4/Li \\ LiNi_{0.5}Mn_{0.5}O_4/Graphite \end{array}$	3.5–5.2 V 3.5–4.6 V	95% after 100 cycles 90% after 100 cycles	[22]
1 M LiFSI/DME-TFEO	NMC811/Li	2.8–4.4 V	80% after 300 cycles	[34]
9.25 M LiTFSI in DMC + 21 M LiTFSI in H ₂ O	$\mathrm{LiNi}_{0.5}\mathrm{Mn}_{1.5}\mathrm{O}_{4}/\mathrm{Li}_{4}\mathrm{Ti}_{5}\mathrm{O}_{12}$	2.0–3.5 V	89.4% after 200 cycles	[53]
4 M LiTFSI-LiDFOB in DME	LiNi _{1/3} Mn _{1/3} Co _{1/3} /Li	2.7–4.3 V	90.5% after 300 cycles	[153]
1.54 M LiFSI in DME-TTE-EC	NMC811/graphite	2.5-4.4 V	98.5% after 500 cycles	[160]
LiFSI+DMC+OTE (molar ratio of 0.51:0.84:0.84)	NMC532/Si-graphite	3.0–4.1 V	76.5% after 300 cycles	[161]

interface. In contrast to typical aqueous solutions, a hydrate melt consisting of lithium salts, where almost all water molecules involve in the hydration process of Li⁺. The lack of free water results in a significantly expanded electrochemical stability window for high-energy aqueous batteries. [143] As shown in Figure 10D, due to the extremely high Li saltto-water molar concentration ratio in the hydrate melt, several unusual physicochemical behaviors were brought out by the absence of the free water molecules. This derived from the strong Coulombic bonding of the oxygen atom in the water molecule by the Li⁺ instead of forming hydrogen bonding networks in such an aqueous electrolyte, leading to the suppression of water hydrolysis and the breakthrough of anodic and cathodic limit. Therefore, as shown in Figure 10C, most electrode materials employed in aprotic electrolyte-based battery systems can be accommodated in such an expanded voltage stability window. Amongst, there achieves the highest voltage aqueous battery of exceeding 3.0 V by coupling Li₄Ti₅O₁₂ anode with LiNi_{0.5}Mn_{1.5}O₄ cathode. As known, a high-quality interphase between electrolyte and electrode not

only changes the electrochemical behaviors of electrolyte solvents and salts to expand electrochemical stability window of electrolyte, but also has an important effect on cycling stability of electrode. Wang et al. reported a new class of electrolytes with an apparent LiTFSI concentration ≈14 M with inherited complementary advantages by mixing aqueous with non-aqueous solvents, where the aqueous portion introduces non-flammability and environmental friendliness characteristic of water-in-salt electrolyte while the aprotic portion brings a secondary ingredient of alkylcarbonate to participate in the formation of the protective interphase on the anode integrated with the LiF deriving from anion reduction by tuning the inner-Helmholtz interfacial structures of the hybridized electrolyte.^[53] As indicated in Figure 10E, this hierarchical interphase pushes the cathodic limit of the hybridized electrolyte down to 1.0 V and extends its anodic limit up to 5.1 V, enabling its 4.1 V electrochemical stability window and a long-term cycling 3.2 V high-energy-density Li-ion cell chemistry constructed on $\text{Li}_4\text{Ti}_5\text{O}_{12}$ and $\text{LiNi}_{0.5}\text{Mn}_{1.5}\text{O}_4$ as shown in Figure 10F. In brief summary, the rational design

1, Downloaded from https://onlinelibrary.wiley.com/do/10,1002/ag2,1.13 by University Town Of Shenzhen, Wiley Online Library for rules of use; OA articles are governed by the applicable Creative Commons. Licenseand Conditions (https://onlinelibrary.wiley.com/erms-and-conditions) on Wiley Online Library for rules of use; OA articles are governed by the applicable Creative Commons. Licenseand Conditions (https://onlinelibrary.wiley.com/erms-and-conditions) on Wiley Online Library for rules of use; OA articles are governed by the applicable Creative Commons. Licenseand Conditions (https://onlinelibrary.wiley.com/erms-and-conditions) on Wiley Online Library for rules of use; OA articles are governed by the applicable Creative Commons. Licenseand Conditions (https://onlinelibrary.wiley.com/erms-and-conditions) on Wiley Online Library for rules of use; OA articles are governed by the applicable Creative Commons. Licenseand Conditions (https://onlinelibrary.wiley.com/erms-and-conditions) on Wiley Online Library for rules of use; OA articles are governed by the applicable Creative Commons. Licenseand Conditions (https://onlinelibrary.wiley.com/erms-and-conditions) on Wiley Online Library for rules of use; OA articles are governed by the applicable Creative Commons. Licenseand Conditions (https://onlinelibrary.wiley.com/erms-and-conditions) on Wiley Online Library for rules of use; OA articles are governed by the applicable Creative Commons.

FIGURE 10 (A,B) Effects of electrolyte concentration on Li⁺ thermodynamic and kinetic behaviors. (A) Change of the equilibrium potential of LiFePO₄ at various electrolyte concentration. In the LiFePO₄ full cells using Li₄Ti₅O₁₂ and Graphite as counter electrode, respectively, the working voltages are about 1.8 V and 3.4 V. E_{ox} and E_{re} refer to the oxidation potential and the reduction potential of free water molecule in the solution with PH = 7. (B) Summary of the main influencing factors on Li⁺ kinetic process on interface. [54] (C,D) The redox potentials of commonly used negative and positive electrode materials in commercial Li batteries originating from either cyclic voltammogram (for Li metal, Mo₆S₈, Li₄Ti₅O₁₂, LiMn₂O₄, and LiFePO₄) or galvanostatic experiments (for the others) with Li⁺/Li potential as correction (C) and the comparisons of electrochemical stability windows based on different aqueous electrolytes with increasing salt-to-water ratios (D). [143] (E,F) The electrochemical performance of the LTO-LNMO full cell. (E) Electrochemical stability window of the hybridized electrolyte deriving from CV measurement on current collectors as well as LTO and LNMO active electrodes. Al and Pt working electrodes are applied for testing cathodic limit and Pt for testing anodic limit, respectively, coupling with activated carbon as counter and Ag/AgCl as reference. (F) Cycling stability and coulombic efficiency when setting a constant current of 6 C to charge and discharge LTO-LNMO full cell. [53]

of Li salt-solvent ratio in aqueous electrolyte would change the hydration structure around Li⁺ centers and the bonding connection between water molecules, which will result in vastly different physicochemical behaviors of electrolyte (e.g., expanded voltage windows for realizing high-energydensity rechargeable aqueous LIBs).

4.2.2 | Li-metal batteries (LMBs)

Exhibiting an ultrahigh theoretical specific capacity (3860 mA h g⁻¹) and extremely low electrode potential (-3.040 V versus standard hydrogen reference electrode), Li metal anode (LMA) has attracted worldwide attention in recent years as it is expected to satisfy the growing demand for high-energy-density Li batteries, especially for its potential applications in Li-oxygen and Li-sulfur batteries, where Li-free cathodes are used. Nevertheless, the progress of its commercialization is severely hindered by extremely poor interfacial stability and safety concerns during cycling, which are associated with interactional factors such as infinite volume changes, Li dendrite formation, and continuous side reactions due to the intrinsic thermodynamics of electrolyte at such a low potential. [30,144,145] Numerous strategies have been proposed and attempted to modify LMA mainly aiming to ensure a uniform Li⁺ flux distributed through interface when charging, finally resulting in dendrite-free Li deposits during repeated Li plating/stripping.^[146] Electrolyte modification is one the most convenient and highly effective method among all improving strategies for LMA. However, commercially used conventional carbonate ester electrolytes with routine Li salt concentration for LIBs were confirmed to have a poor interfacial compatibility against LMA due to the intrinsic thermodynamic instability of free solvent molecules, leading to the formation of poor SEI with most alkyl lithium carbonate-like organic species, which fails to guide the uniform Li⁺ flux and is insufficient to tolerate huge volume change of LMA during repeated Li plating/stripping.^[147,148] As mentioned above, high-voltage cathodes for high-energy-density LMBs are also incompatible with conventional dilute carbonate ester electrolytes under high cut-off voltages.^[149,150] Suo et al.^[27] reported that Li+ transference number in HCE was higher than that in dilute electrolyte. This enables Li⁺ to have a higher mass transfer flux, which is conducive to the uniform substance exchange at the interface of LMA; at the same time, it can effectively suppress the space charge layer generated by the consumption of interface anions, thereby reducing the electric field drive force of the non-uniform deposition of metal lithium. Therefore, to be clear, reorganizing the Li⁺ solvation sheath with more anions involved and decreasing available free solvent molecules to lower their reduction and oxidation activities in the solution should be effective to guide the decomposition reactions on the interfaces to reconstruct mechanically and electrochemically desirable SEIs and CEIs with a higher content of inorganic species, which can be easily achieved by the utilization of HCEs.[151] Figure 11A compares the difference in the formation process of CEI on cathode between dilute and concentrated electrolytes.[152] In the traditional dilute electrolyte, dominated free solvents preferentially reduce to form a carbonate-derived CEI, which is rich in organic species. This CEI is insufficient to protect

the cathode from further attacking due to its fragile and nonuniform characteristics. However, in HCEs, the dominant LiPF₆ tends to decompose and participate in the formation of anion-derived CEI, making it LiF-rich. Such CEI composition is believed to be strong, uniform, and dense, so that it is helpful to protect cathodes and suppress the dissolution of transition metals, leading to excellent electrochemical performance of LMBs. Compared to carbonic ester electrolytes, ether-based electrolytes are relatively unstable against oxidation, which leads to their incompatibility when operated at a charging cut-off voltage above 4.0 V (vs. Li). Therefore, ether-based electrolytes are not widely considered for the use in high-voltage LMBs despite their better reduction stability against LMAs. Jiao et al. designed a dual-salt-based HCE with ethers as solvents to exhibit superior oxidation stability to enable more stable cycling performance of ternary cathode materials-based LMB with a charge cut-off voltage up to 4.3 V, as displayed in Figure 11B.[153] The reasons behind this are that the reorganized solution structure of HCE plays an important role in intensifying the oxidation stability of ether molecules since there rarely exists free solvent molecule and induces the formation of more stable anion-derived interfacial layers on both cathode and anode by synergetic effects of dual salts, which can effectively passivate the NMC cathode surface with highly catalytic activity at high operation voltage, as well as simultaneously helping form a high-quality SEI layer on the LMA for efficient Li plating and stripping without dendrite formation. Cao et al. proposed a fluorinated orthoformate solvent-based LHCE for LMBs, which formed a monolithic, homogeneous, and inorganic rich SEI on Li anode, which ensures uniform Li deposition. As a result, interfacial Li depletion and electrode pulverization can be avoided (Figure 11D-G), consequently leading to high Coulombic efficiency for metallic Li anodes. For instance, as shown in Figure 11C, after adding tris(2,2,2trifluoroethyl)orthoformate (TFEO), which exhibits low HOMO value and good Li metal compatibility ether groups, as a diluent to prepare an LHCE, the cyclic stability of high-voltage Li||NMC811 LMB is dramatically improved due to the better interfacial stability at both electrodes.^[34] Based on these findings, it is demonstrated that by regulating the structure and composition of the Li⁺ solvation sheath via HCE/LHCE preparation, high-quality interfaces can be constructed in high-voltage LMBs. Additionally, it has been also demonstrated that HCE can also be applied to suppress the dissolution and shuttle effect of polysulfide to stop deteriorating LMA and enable Li-S batteries.[154,155]

4.2.3 | Traditional LIBs

To approach commercial requirements for high-energy-density LIBs, one pragmatic strategy is to develop cathode materials with high operating voltage. However, in such scenarios, severe transition metal dissolution and corrosion of the Al current collector cannot be solved simultaneously by using conventional LiPF₆ salt-based carbonic ester electrolytes. Therefore, it is critical to further address abovementioned issues by creating a better interfacial protection layer. Wang et al. reported a DMC-based electrolyte with high concentrations of LiN(SO₂F)₂ (LiFSA) for a 5 V-class LiNi_{0.5}Mn_{1.5}O₄/graphite battery exhibiting excellent rate

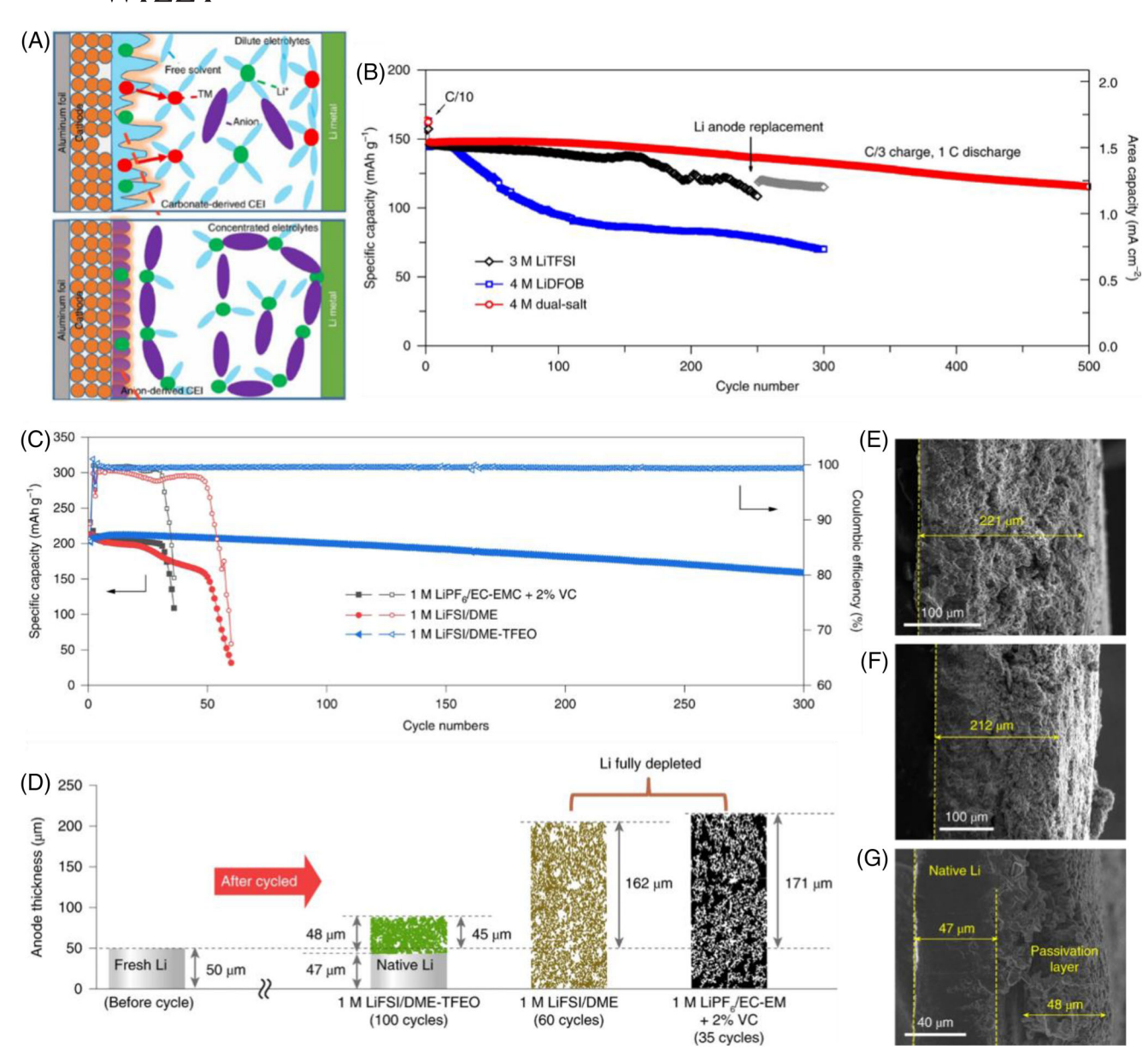


FIGURE 11 (A) Schematic illustrations of the formation process of passivation films on cathode in dilute and concentrated electrolytes, respectively. [152] (B) The comparisons of cycling stability of Li|NMC cells when cycled with different highly concentrated DME-based electrolytes using different salts and concentrations. [153] (C–G) Cycling performances of Li|NMC811 cells using different investigated electrolytes (C) and Li depletion, pulverization, and volumetric expansion after cycled and retrieved from Li|NMC811 cells (D–G). (D) Schematic illustrations of Li consumption and corresponding volumetric expansion after cycled in different electrolytes; the cell using electrolyte of 1 M LiFSI in DME-TFEO exhibits extremely stable cycling performance and shows minimal volume change of LMA even after 100 cycles, while the cells using electrolyte comprising of 1 M LiPF₆ in EC/EMC with 2% VC and 1 M LiFSI in DME failed sooner at earlier stage of 35th and 60th cycle, respectively, due to the complete Li depletion and accumulation of inactive species on the surface of LMA. (E–G) SEM images by cross-section views of LMA cycled in the electrolytes of 1 M LiPF₆/EC-EMC+2% VC (E), 1 M LiFSI/DME (F), and 1 M LiFSI/DME-TFEO (G)^[34]

and cycling performance. [22] As shown in Figure 12A, improved oxidation stability towards Al current collector of the electrolyte can be achieved with the increasing salt-to-solvent ratios. It is believed that a peculiar 3D network of anions and solvent molecules coordinated strongly to Li⁺ centers contributes the improved electrochemical behaviors. Besides, HCEs were also demonstrated to have a significant impact on the anode performance in high-energy-density LIBs by inhibiting solvent co-intercalation and improving the fast-charging performance of graphite anode. [156,157] Owing to the high theoretical capacity, Si-based anodes are the most promising next-generation anode materials for high-performance LIBs. However, excessive growth of SEIs caused by the huge volume change severely damaged the

cyclability of Si anodes. Tuning electrolyte properties such as salt concentration for a more stable SEI with self-limiting property, which is expected to mitigate these problems. [158] Chang et al. designed a super-concentrated LiFSI-based PC electrolyte for long-term cycling performance of silicon nanoparticles. [159] As compared in Figure 12B–D, with the increasing concentrations of LiFSI salt in PC solvent, the size of the cracks observed in the surface of silicon nanoparticle electrode after 50 cycles minimizes to low level without running through the walls and aggregation of the irregularly small particles. The authors demonstrated this phenomenon derived from the formation of a chemically stable and mechanically robust complex SEI layer on the surface of silicon nanoparticles to resist the deformation,

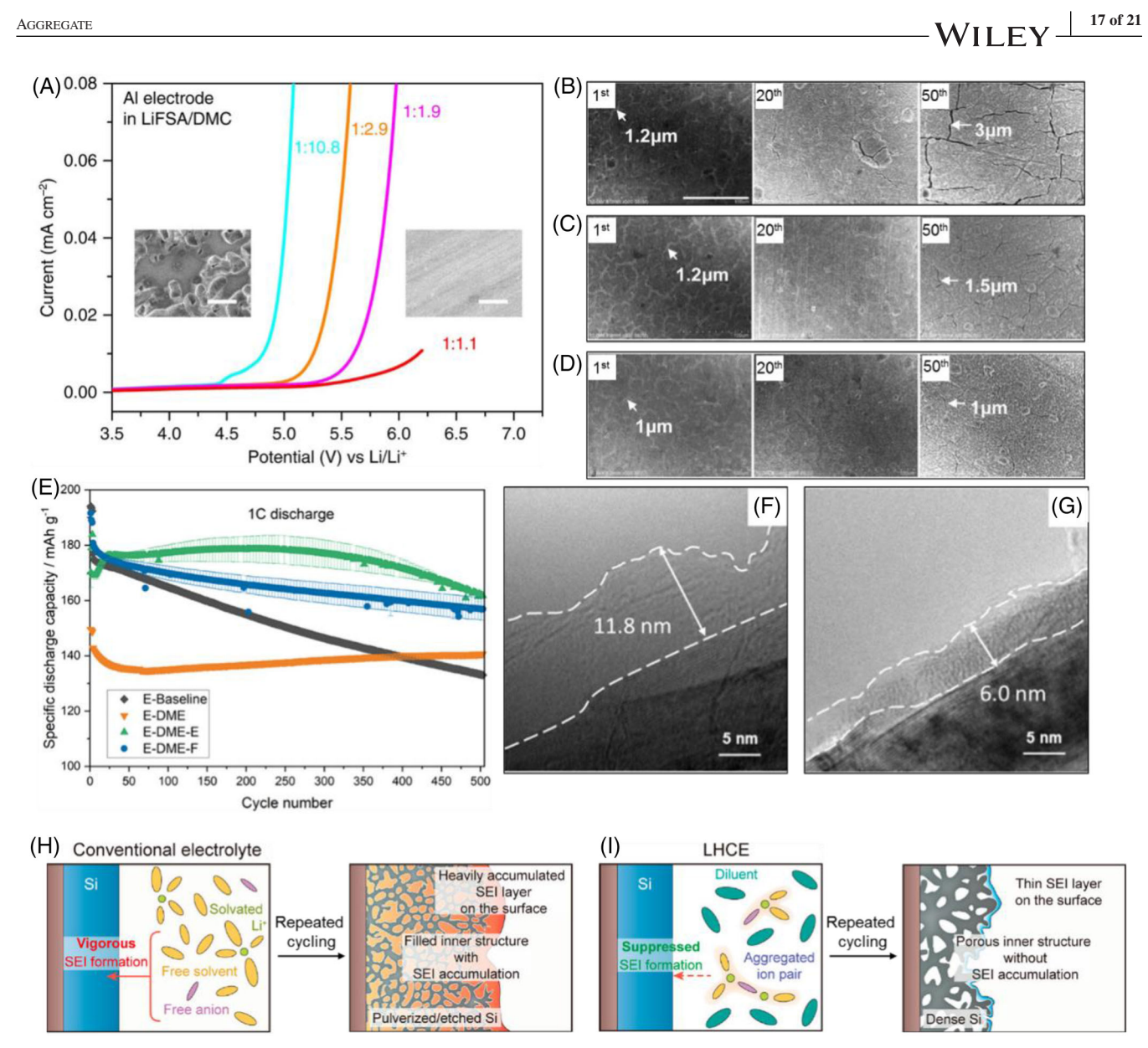


FIGURE 12 (A) LSV of LiFSA/DMC electrolytes with various salt concentrations against Al electrode measured in a three-electrode cell. The SEM image inset in the left of panel shows the surface of Al electrode with many corroding pits due to a severe anodic Al corrosion when polarized in the dilute electrolyte of 1:10.8, while the SEM image inset in the right of panel displays the surface of Al electrode without corroding pits found due to a good inhibition of anodic Al corrosion when polarized in super-concentrated electrolyte of 1:1.1.^[22] (B–D) FE-SEM images for investigating the evolution of surface morphology of silicon nanoparticle electrodes cycled in the electrolytes of LiFSI-(PC)₈ (B), LiFSI-(PC)₃ (C), and LiFSI-(PC)₂ (D), respectively, for different cycle number (1, 20, and 50). [159] (E-G) Cycling stability of Gr||NMC811 cells with different electrolytes (E) and interfacial structures and morphologies on Gr particles after cycled in conventional electrolyte (E-baseline) (F) and LHCE (E-DME-F) (G).[160] (H-I) Schemes illustrate the effects of the conventional electrolyte (H) and LHCE (I) on the formation and degradation of interfacial structure on Si anodes [161]

hence the better structural integrity of bulk silicon nanoparticles. It was found that this "high-quality" SEI depended on the formation of a specific fluid polymeric network-like solution structure, where more FSI⁻ was reduced to form the dominant SEI component with elevated salt concentrations in the electrolyte. Jia et al. developed DME-based LHCEs with TTE as a diluent and appropriate electrolyte additives to facilitate high-energy-density NMC811||Gr LIB.^[160] It is clear to be observed in Figure 12F-G that an effective salt anion-derived SEI as an intact protection layer is covered on the Gr anode, which is regulated by the unique microscopic coordination structure formed in DME-based LHCEs where most LiFSI exist as nondissociated ion pairs. Therefore, these LHCEs with finely tuned structure and composition of solvation sheaths and a highly beneficial synergetic effect of electrolyte additive well solve the problems of co-intercalation into Gr as well as anodic instability at high voltages. Hence, excellent rate capability and capacity retention after long-term cycling can be achieved for Gr|NMC811 cells even at 4.4 V (Figure 12E). Chae et al. designed a DMC-based LHCE, where 1H,1H,5H-octafluoropentyl 1,1,2,2-tetrafluoroethyl ether (OTE) was selected as a diluent to facilitate a tailored structure on Si anode to improve its long-term cycling performance at both room and high temperatures.^[161] As illustrated in Figure 12H,I, based on conventional carbonic ester electrolyte, the SEI formed on the Si anode is thick and fragile, leading to its heavy accumulation on the surface and inner structure during repeated cycling. As a result, the Si anode is pulverized and etched. In comparison, the Si anode cycled in the OTE-based LHCE exhibits a thin SEI with higher mechanical strength. This is attributed to the optimized the salt-solvent complex structure

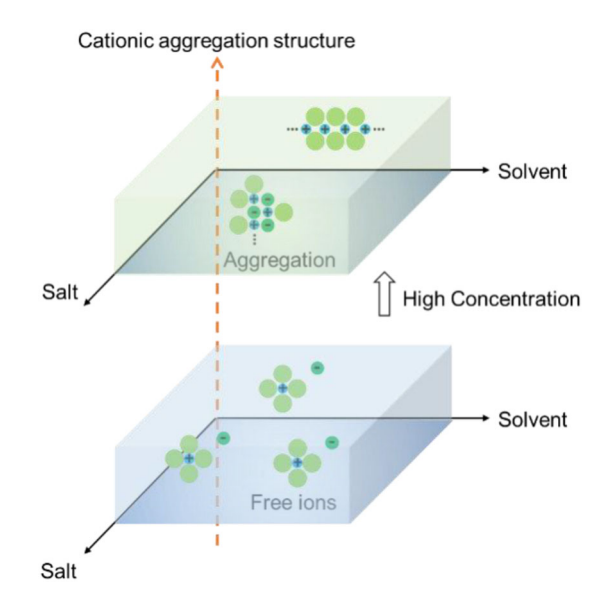


FIGURE 13 Three dimensional electrolyte design concept, including dilute electrolyte and concentrated electrolyte

with an OTE diluent, which promotes the decomposition of LiFSI, so that the dense structure of Si after long-term cycling is preserved without surface etching and thick SEI formation. As a result, improved cycle life of Si anodes is realized over a wide temperature range. In summary, benefiting from the unique ion solvation structure in the HCE by mixing more Li salt and less solvent for modified physicochemical properties and associated anion-dominant interfacial formation mechanism instead of solvent decomposition process, many conventional carbonic esters-based electrolytes that previously demonstrated to be unstable anodes and cathodes are expected to be reconsidered for implementation in high safety, high specific energy, and long-life LIBs.

5 | CONCLUSION AND PERSPECTIVE

Here, we first summarized the techniques on characterizing electrolyte structure characterization, and deeply studied the relationship between electrolyte coordination structure and cell performance, including dilute electrolyte, HCE, and LHCE. In structural dimension, the pros and cons of the applied electrolytes were dissected, such as in concentrated electrolyte, new functionalities on stabilizing interface structure and extending battery life are obtained by its cationic aggregation structure in the absence of free solvent molecules and the extensive formation of ion pairs. Nevertheless, higher viscosity and lower ionic conductivity compared to the dilute solution are also resulted. The emerging electrolyte design of LHCE is based on the complementary advantages of dilute and HCE, achieving promising results in many battery systems. Accordingly, we proposed a three-dimensional electrolyte design strategy, including salt, solvent, and cationic aggregation structure, to be referred for exploring next breakthroughs in battery electrolytes as displayed in Figure 13. This design strategy is not just a conclusion based on the previous literatures, but a milestone position for future electrolyte exploration. With novel theoretical calculation tools for predictions and rational designs as well as advanced characterization techniques for

verification, a new electrolyte era is expected and the faced issues in conventional electrolyte system can be resolved eventually.

Despite the exciting progresses made in developing electrolytes in the past decades, below, some scientific and engineering challenges and, most importantly, future research directions of electrolytes for LIBs are listed. We believe that continuous worldwide efforts in both academic and industry areas will enable the next-generation high-energy Li batteries in the near future.

- 1. For dilute electrolytes, the addition of special solvents and/or additives could be the most effective way to regulate the coordination structures. Future efforts should be devoted to screen and synthesize compounds which are prone to be coordinated with cation and transferred to the electrode surface for constructing a stable electrodeelectrolyte interface to promote interfacial charge transfer kinetics and suppress side reactions. [162] Or, introducing some solvents which are easier to be decomposed than the applied main solvents to protect solid-liquid interface. To achieve this goal, computational approaches (e.g., classical and first-principle MD simulations) might be helpful. Moreover, when we obtain the coordination ability of cation with various solvents, we can design the solution structure according to these coordination information, for example, in multiple solvents electrolyte, the composition proportion can be reasonably calculated to achieve the optimal performance.
- 2. Concentrated electrolytes, including HCEs and LHCEs with cation aggregation solution structures, experienced unprecedented development these years. However, the corresponding safety issues have not been well studied, especially for the emerging LHCE, which contains plenty of diluent presenting low volatilization temperature. Hence, in HCEs and LHCEs systems, appropriate flame-retardant can be chosen to further improve their comprehensive performances when operated at extreme conditions and eliminate safety concerns. For example, the combination of high concentration aqueous electrolyte and organic dilute solution, which is expected to enhance the battery safety. Besides, it is wise to screen or synthesis some organic diluents with high boiling points and nonflammability. Overall, LHCEs seem to be a very promising and ideal electrolyte systems which would be compatible with most of the prevailing Li battery systems to pursue higher energy and power densities if the faced issues can be properly solved.
- The cost and environmental unfriendliness of highly fluorinated concentrated electrolytes have also impeded their practical application. Therefore, it would be of great importance to investigate concentrated electrolytes with lower F contents.
- 4. The concept established in Li⁺-based electrolytes might be extended or transferred to other alkaline metal ionbased and multi-valent ion-based electrolyte systems as a technical reserve for post-Li systems as they might be facing similar scientific challenges.

ACKNOWLEDGMENTS

This work was financially supported by the Chemistry and Chemical Engineering Guangdong Laboratory (Grant

No.1922018) and Soft Science Research Project of Guangdong Province (No. 2017B030301013).

CONFLICT OF INTEREST

The authors declare no conflict of interest.

ETHICS STATEMENT

The authors declare no ethics issue.

DATA AVAILABILITY STATEMENT

Data is available, please reach to Jiangtao Hu (hujiangtao 89@qq.com).

ORCID

Guorui Zheng https://orcid.org/0000-0003-0277-7983 *Feng Pan* https://orcid.org/0000-0002-8216-1339

REFERENCES

- 1. K. Xu, Chem. Rev. 2004, 104, 4303.
- 2. M. S. Whittingham, Science 1976, 192, 1126.
- 3. W. R. McKinnon, J. R. Dahn, J. Electrochem. Soc. 1985, 132, 364.
- R. Fong, U. von Sacken, J. R. Dahn, J. Electrochem. Soc. 1990, 137, 2009.
- 5. M. S. Whittingham, Proc. Inst. Electr. Electron. Eng. 2012, 100, 1518.
- 6. M. S. Dresselhaus, I. L. Thomas, Nature 2001, 414, 332.
- 7. M. Armand, J. M. Tarascon, Nature 2008, 451, 652.
- G. Harper, R. Sommerville, E. Kendrick, L. Driscoll, P. Slater, R. Stolkin, A. Walton, P. Christensen, O. Heidrich, S. Lambert, A. Abbott, K. Ryder, L. Gaines, P. Anderson, *Nature* 2019, 575, 75.
- 9. Y. Liu, Y. Zhu, Y. Cui, Nat. Energy 2019, 4, 540.
- 10. W. Li, J. R. Dahn, D. S. Wainwright, Science 1994, 264, 1115.
- L. Suo, O. Borodin, T. Gao, M. Olguin, J. Ho, X. Fan, C. Luo, C. Wang, K. Xu, Science 2015, 350, 938.
- D. Kundu, B. D. Adams, V. Duffort, S. H. Vajargah, L. F. Nazar, *Nat. Energy* 2016, 1, 16119.
- H. Kim, J. Hong, K.-Y. Park, H. Kim, S.-W. Kim, K. Kang, Chem. Rev. 2014, 114, 11788.
- 14. F. Beck, P. Rüetschi, Electrochim. Acta 2000, 45, 2467.
- 15. J.-Y. Luo, W.-J. Cui, P. He, Y.-Y. Xia, Nat. Chem. 2010, 2, 760.
- G. J. Wang, L. C. Yang, Q. T. Qu, B. Wang, Y. P. Wu, R. Holze, J. Solid State Electrochem. 2010, 14, 865.
- 17. M. S. Whittingham, Chem. Rev. 2014, 114, 11414.
- J. Liu, Z. Bao, Y. Cui, E. J. Dufek, J. B. Goodenough, P. Khalifah, Q. Li, B. Y. Liaw, P. Liu, A. Manthiram, Y. S. Meng, V. R. Subramanian, M. F. Toney, V. V. Viswanathan, M. S. Whittingham, J. Xiao, W. Xu, J. Yang, X.-Q. Yang, J.-G. Zhang, Nat. Energy 2019, 4, 180.
- H.-H. Ryu, K.-J. Park, C. S. Yoon, Y.-K. Sun, Chem. Mater. 2018, 30, 1155.
- J.-S. Kim, C. S. Johnson, J. T. Vaughey, M. M. Thackeray, S. A. Hackney, W. Yoon, C. P. Grey, *Chem. Mater.* 2004, 16, 1996.
- J. Lee, A. Urban, X. Li, D. Su, G. Hautier, G. Ceder, Science 2014, 343, 519.
- J. Wang, Y. Yamada, K. Sodeyama, C. H. Chiang, Y. Tateyama, A. Yamada, Nat. Commun. 2016, 7, 12032.
- X. Fan, L. Chen, X. Ji, T. Deng, S. Hou, J. Chen, J. Zheng, F. Wang, J. Jiang, K. Xu, C. Wang, *Chem* 2018, 4, 174.
- J. Zheng, G. Tan, P. Shan, T. Liu, J. Hu, Y. Feng, L. Yang, M. Zhang, Z. Chen, Y. Lin, J. Lu, J. C. Neuefeind, Y. Ren, K. Amine, L.-W. Wang, K. Xu, F. Pan, Chem 2018, 4, 2872.
- 25. S. Ko, Y. Yamada, A. Yamada, Batter. Supercaps 2020, 3, 910.
- D. W. McOwen, D. M. Seo, O. Borodin, J. Vatamanu, P. D. Boyle, W. A. Henderson, *Energy Environ. Sci.* 2014, 7, 416.
- L. Suo, Y.-S. Hu, H. Li, M. Armand, L. Chen, *Nat. Commun.* 2013, 4, 1481.
- S. Hwang, D.-H. Kim, J. H. Shin, J. E. Jang, K. H. Ahn, C. Lee, H. Lee, J. Phys. Chem. C 2018, 122, 19438.
- P. Shi, H. Zheng, X. Liang, Y. Sun, S. Cheng, C. Chen, H. Xiang, *Chem. Commun.* 2018, 54, 4453.
- W. Xu, J. Wang, F. Ding, X. Chen, E. Nasybulin, Y. Zhang, J.-G. Zhang, Energy Environ. Sci. 2014, 7, 513.

- K. Matsumoto, K. Inoue, K. Nakahara, R. Yuge, T. Noguchi, K. Utsugi, J. Power Sources 2013, 231, 234.
- J.-G. Zhang, W. Xu, J. Xiao, X. Cao, J. Liu, Chem. Rev. 2020, 120, 13312.
- S. Chen, J. Zheng, D. Mei, K. S. Han, M. H. Engelhard, W. Zhao, W. Xu, J. Liu, J.-G. Zhang, *Adv. Mater.* 2018, *30*, 1706102.
- X. Cao, X. Ren, L. Zou, M. H. Engelhard, W. Huang, H. Wang, B. E. Matthews, H. Lee, C. Niu, B. W. Arey, Y. Cui, C. Wang, J. Xiao, J. Liu, W. Xu, J.-G. Zhang, *Nat. Energy* 2019, 4, 796.
- X. Cao, H. Jia, W. Xu, J.-G. Zhang, J. Electrochem. Soc. 2021, 168, 010522.
- A. K. Padhi, K. S. Nanjundaswamy, J. B. Goodenough, J. Electrochem. Soc. 1997, 144, 1188.
- Y. Duan, B. Zhang, J. Zheng, J. Hu, J. Wen, D. J. Miller, P. Yan, T. Liu, H. Guo, W. Li, X. Song, Z. Zhuo, C. Liu, H. Tang, R. Tan, Z. Chen, Y. Ren, Y. Lin, W. Yang, C.-M. Wang, L.-W. Wang, J. Lu, K. Amine, F. Pan, Nano Lett. 2017, 17, 6018.
- K. Mizushima, P. C. Jones, P. J. Wiseman, J. B. Goodenough, *Mater. Res. Bull.* 1980, 15, 783.
- J. Hu, Q. Wang, B. Wu, S. Tan, Z. Shadike, Y. Bi, M. S. Whittingham,
 J. Xiao, X.-Q. Yang, E. Hu, ACS Appl. Mater. Inter. 2021, 13, 2622.
- M. M. Thackeray, W. I. F. David, P. G. Bruce, J. B. Goodenough, *Mater. Res. Bull.* 1983, 18, 461.
- T. Liu, A. Dai, J. Lu, Y. Yuan, Y. Xiao, L. Yu, M. Li, J. Gim, L. Ma, J. Liu, C. Zhan, L. Li, J. Zheng, Y. Ren, T. Wu, R. Shahbazian-Yassar, J. Wen, F. Pan, K. Amine, *Nat. Commun.* 2019, 10, 4721.
- 42. K. Xu, Chem. Rev. 2014, 114, 11503.
- 43. X. Fan, C. Wang, Chem. Soc. Rev. 2021, 50, 10486.
- 44. O. Borodin, J. Self, K. A. Persson, C. Wang, K. Xu, Joule 2020, 4, 69.
- W. Zhou, M. Zhang, X. Kong, W. Huang, Q. Zhang, Adv. Sci. 2021, 8, 2004490.
- H. J. Liang, Z. Y. Gu, X. X. Zhao, J. Z. Guo, J. L. Yang, W. H. Li, B. Li, Z. M. Liu, W. L. Li, X. L. Wu, *Angew. Chem. Int. Ed.* 2021, 60, 26837.
- X. K. Hou, S. F. Li, W. H. Li, H. J. Liang, Z. Y. Gu, X. X. Luo, X. L. Wu, Batter. Supercaps 2021, 4, 1647.
- 48. S. Guo, L. Qin, T. Zhang, M. Zhou, J. Zhou, G. Fang, S. Liang, *Energy Storage Mater.* **2021**, *34*, 545.
- J. Vatamanu, O. Borodin, G. D. Smith, J. Phys. Chem. C 2012, 116, 1114
- S. Chen, J. Zheng, D. Mei, K. S. Han, M. H. Engelhard, W. Zhao, W. Xu, J. Liu, J. G. Zhang, *Adv. Mater.* 2018, *30*, 1706102.
- S.-K. Jeong, M. Inaba, Y. Iriyama, T. Abe, Z. Ogumi, Electrochem. Solid-State Lett. 2003, 6, A13.
- Y. Yamada, Y. Takazawa, K. Miyazaki, T. Abe, J. Phys. Chem. C 2020, 114, 11680.
- F. Wang, O. Borodin, M. S. Ding, M. Gobet, J. Vatamanu, X. Fan, T. Gao, N. Eidson, Y. Liang, W. Sun, S. Greenbaum, K. Xu, C. Wang, Joule 2018, 2, 927.
- J. Hu, H. Guo, Y. Li, H. Wang, Z. Wang, W. Huang, L. Yang, H. Chen,
 Y. Lin, F. Pan, *Nano Energy* 2021, 89, 106413.
- J. Hu, W. Ren, X. Chen, Y. Li, W. Huang, K. Yang, L. Yang, Y. Lin, J. Zheng, F. Pan, *Nano Energy* 2020, 74, 104864.
- S. R. Galle Kankanamge, D. G. Kuroda, J. Phys. Chem. B 2020, 124, 1965.
- 57. J. Mähler, I. Persson, Inorg. Chem. 2012, 51, 425.
- 58. K. Qian, R. E. Winans, T. Li, Adv. Energy Mater. 2021, 11, 2002821.
- 59. S. Schantz, L. M. Torell, J. R. Stevens, J. Appl. Phys. 1988, 64, 2038.
- D. Battisti, G. A. Nazri, B. Klassen, R. Aroca, J. Phys. Chem. 1993, 97, 5826.
- Z. Wang, B. Huang, H. Huang, R. Xue, L. Chen, F. Wang, J. Electrochem. Soc. 1996, 143, 1510.
- K. Kondo, M. Sano, A. Hiwara, T. Omi, M. Fujita, A. Kuwae, M. Iida, K. Mogi, H. Yokoyama, *J. Phys. Chem. B* 2000, 104, 5040.
- R. Aroca, M. Nazri, G. A. Nazri, A. J. Camargo, M. Trsic, J. Solution Chem. 2000, 29, 1047.
- M. Chabanel, D. Legoff, K. Touaj, J. Chem. Soc. Faraday Trans. 1996, 92, 4199.
- L. Doucey, M. Revault, A. Lautié, A. Chaussé, R. Messina, Electrochim. Acta 1999, 44, 2371.
- S. Petrucci, M. C. Masiker, E. M. Eyring, J. Solution Chem. 2008, 37, 1031
- M. Salomon, M. Xu, E. M. Eyring, S. Petrucci, J. Phys. Chem. C 1994, 98, 8234.

- Y. Yamada, K. Furukawa, K. Sodeyama, K. Kikuchi, M. Yaegashi, Y. Tateyama, A. Yamada, J. Am. Chem. Soc. 2014, 136, 5039.
- 69. Y.-H. Zhang, C. K. Chan, J. Phys. Chem. A 2003, 107, 5956.
- Y. Li, Z. Zhou, W. Deng, C. Li, X. Yuan, J. Hu, M. Zhang, H. Chen,
 R. Li *ChemElectroChem* 2021, 8, 1451.
- H. Watanabe, N. Arai, E. Nozaki, J. Han, K. Fujii, K. Ikeda, T. Otomo, K. Ueno, K. Dokko, M. Watanabe, Y. Kameda, Y. Umebayashi, J. Phys. Chem. B 2021, 125, 7477.
- T. Tsurumura, Y. Hashimoto, M. Morita, Y. Umebayashi, K. Fujii, Anal. Sci. 2019, 35, 289.
- D. M. Seo, O. Borodin, S.-D. Han, P. D. Boyle, W. A. Henderson, J. Electrochem. Soc. 2012, 159, A1489.
- 74. R. M. Hochstrasser, PNAS 2007, 104, 14189.
- 75. B. M. Auer, J. L. Skinner, J. Chem. Phys. 2008, 128, 224511.
- K. D. Fulfer, D. G. Kuroda, Phys. Chem. Chem. Phys. 2017, 19, 25140.
- 77. J. Barthel, R. Buchner, E. Wismeth, J. Sol. Chem. 2000, 29, 937.
- D. M. Seo, S. Reininger, M. Kutcher, K. Redmond, W. B. Euler, B. L. Lucht, J. Phys. Chem. C 2015, 119, 14038.
- 79. K. D. Fulfer, D. G. Kuroda, J. Phys. Chem. C 2016, 120, 24011.
- M. G. Giorgini, K. Futamatagawa, H. Torii, M. Musso, S. Cerini, J. Phys. Chem. Lett. 2015, 6, 3296.
- M. T. Ong, O. Verners, E. W. Draeger, A. C. T. van Duin, V. Lordi, J. E. Pask, J. Phys. Chem. B 2015, 119, 1535.
- B. Fortunato, P. Mirone, G. Fini, Spectrochim. Acta A Mol. Biomol. Spectrosc. 1971, 27, 1917.
- 83. J. R. Durig, J. W. Clark, J. M. Casper, J. Mol. Struc. 1970, 5, 67.
- 84. J. T. Arnold, M. E. Packard, J. Chem. Phys. 1951, 19, 1608.
- 85. S. R. Dillon, R. C. Dougherty, J. Phys. Chem. A 2003, 107, 10217.
- X. Bogle, R. Vazquez, S. Greenbaum, A. v. W. Cresce, K. Xu, J. Phys. Chem. Lett. 2013, 4, 1664.
- C. Wan, M. Y. Hu, O. Borodin, J. Qian, Z. Qin, J.-G. Zhang, J. Z. Hu, J. Power Sources 2016, 307, 231.
- X. Deng, M. Y. Hu, X. Wei, W. Wang, Z. Chen, J. Liu, J. Z. Hu, J. Power Sources 2015, 285, 146.
- K. Hayamizu, K. Sugimoto, E. Akiba, Y. Aihara, T. Bando, W. S. Price, J. Phys. Chem. B 2002, 106, 547.
- 90. L. Yang, A. Xiao, B. L. Lucht, J. Mol. Liq. 2010, 154, 131.
- F. Castiglione, A. Baggioli, A. Citterio, A. Mele, G. Raos, J. Phys. Chem. A 2012, 116, 1814.
- I. Ruggeri, A. La Monaca, F. De Giorgio, F. Soavi, C. Arbizzani, V. Berbenni, C. Ferrara, P. Mustarelli, *ChemElectroChem* 2019, 6, 4002.
- 93. A. Guinier, Nature 1938, 142, 569.
- 94. Z. Feng, E. Sarnello, T. Li, L. Cheng, *J. Electrochem. Soc.* **2019**, *166*,
- L. Aguilera, S. Xiong, J. Scheers, A. Matic, J. Mol. Liq. 2015, 210, 238.
- S. Saito, H. Watanabe, K. Ueno, T. Mandai, S. Seki, S. Tsuzuki, Y. Kameda, K. Dokko, M. Watanabe, Y. Umebayashi, J. Phys. Chem. B 2016, 120, 3378.
- Z. Yu, L. A. Curtiss, R. E. Winans, Y. Zhang, T. Li, L. Cheng, J. Phys. Chem. Lett. 2020, 11, 1276.
- O. Borodin, L. Suo, M. Gobet, X. Ren, F. Wang, A. Faraone, J. Peng, M. Olguin, M. Schroeder, M. S. Ding, E. Gobrogge, A. von Wald Cresce, S. Munoz, J. A. Dura, S. Greenbaum, C. Wang, K. Xu, ACS Nano 2017, 11, 10462.
- F. Dommert, K. Wendler, R. Berger, L. Delle Site, C. Holm, Chemphyschem 2012, 13, 1625.
- N. N. Rajput, V. Murugesan, Y. Shin, K. S. Han, K. C. Lau, J. Chen, J. Liu, L. A. Curtiss, K. T. Mueller, K. A. Persson, *Chem. Mater.* 2017, 29, 3375.
- 101. I. Pethes, J. Mol. Liq. 2017, 242, 845.
- 102. C. Schroder, Phys. Chem. Chem. Phys. 2012, 14, 3089.
- D. Bedrov, J. P. Piquemal, O. Borodin, A. D. MacKerell Jr., B. Roux, C. Schroder, *Chem. Rev.* 2019, 119, 7940.
- 104. S. Patel, C. L. Brooks, Mol. Simul. 2006, 32, 231.
- 105. H. Yu, W. F. van Gunsteren, Comput. Phys. Commun. 2005, 172, 69.
- 106. S. V. Levchenko, A. I. Krylov, J. Chem. Phys. 2004, 120, 175.
- X. Wang, F. Chen, G. M. A. Girard, H. Zhu, D. R. MacFarlane, D. Mecerreyes, M. Armand, P. C. Howlett, M. Forsyth, *Joule* 2019, 3, 2687.
- 108. F. Chen, P. Howlett, M. Forsyth, J. Phys. Chem. C 2017, 122, 105.
- C. V. Amanchukwu, Z. Yu, X. Kong, J. Qin, Y. Cui, Z. Bao, J. Am. Chem. Soc. 2020, 142, 7393.

- J. Wang, Y. Yamada, K. Sodeyama, C. H. Chiang, Y. Tateyama, A. Yamada, Nat. Commun. 2016, 7, 12032.
- H. Jia, P. Gao, L. Zou, K. S. Han, M. H. Engelhard, Y. He, X. Zhang,
 W. Zhao, R. Yi, H. Wang, C. Wang, X. Li, J.-G. Zhang, *Chem. Mater.* 2020, 32, 8956.
- S. J. L. Billinge, Philos. Trans. A Math. Phys. Eng. Sci. 2019, 377, 20180413.
- T. Yamaguchi, K. Yoshida, T. Yamaguchi, Y. Kameda, K. Ikeda, T. Otomo, J. Phys. Chem. B 2017, 121, 5355.
- 114. G. Mao, M. Saboungi, D. Price, Phys. Rev. Lett. 2000, 84, 5536.
- 115. W. Rudolph, M. H. Brooker, C. C. Pye, J. Phys. Chem. 1995, 99, 3793.
- 116. C. C. Pye, W. Rudolph, R. A. Poirier, J. Phys. Chem. 1996, 100, 601.
- 117. H. H. Loeffler, B. M. Rode, J. Chem. Phys. 2002, 117, 110.
- 118. S. Yanase, T. Oi, J. Nucl. Sci. Technol. 2002, 39, 1060.
- 119. Y. Yamada, Electrochemistry 2017, 85, 559.
- R. Fong, U. von Sacken, J. R. Dahn, J. Electrochem. Soc. 1990, 137, 2009.
- 121. S. S. Zhang, K. Xu, T. R. Jow, J. Power Sources 2006, 159, 702.
- L. Liao, X. Cheng, Y. Ma, P. Zuo, W. Fang, G. Yin, Y. Gao, *Electrochim. Acta* 2013, 87, 466.
- X. Ma, R. Young, L. Ellis, L. Ma, J. Li, J. Dahn, J. Electrochem. Soc. 2019, 166, A2665.
- 124. J. Hu, L. Li, E. Hu, S. Chae, H. Jia, T. Liu, B. Wu, Y. Bi, K. Amine, C. Wang, J. Zhang, J. Tao, J. Xiao, *Nano Energy* 2021, 79, 105420.
- W. Song, J. Harlow, E. Logan, H. Hebecker, M. Coon, L. Molino, M. Johnson, J. Dahn, M. Metzger, J. Electrochem. Soc. 2021, 168, 090503.
- D. Ruan, M. Chen, X. Wen, S. Li, X. Zhou, Y. Che, J. Chen, W. Xiang,
 S. Li, H. Wang, X. Liu, W. Li, *Nano Energy* 2021, 90, 106535.
- 127. J. Zheng, Y. Hou, Y. Duan, X. Song, Y. Wei, T. Liu, J. Hu, H. Guo, Z. Zhuo, L. Liu, Z. Chang, X. Wang, D. Zherebetskyy, Y. Fang, Y. Lin, K. Xu, L.-W. Wang, Y. Wu, F. Pan, *Nano Lett.* 2015, 15, 6102.
- J. Hu, Y. Jiang, S. Cui, Y. Duan, T. Liu, H. Guo, L. Lin, Y. Lin, J. Zheng, K. Amine, F. Pan, *Adv. Energy Mater.* 2016, 6, 1600856.
- C. Yan, H.-R. Li, X. Chen, X.-Q. Zhang, X.-B. Cheng, R. Xu, J.-Q. Huang, Q. Zhang, J. Am. Chem. Soc. 2019, 141, 9422.
- G. V. Zhuang, K. Xu, H. Yang, T. R. Jow, P. N. Ross, J. Phys. Chem. B 2005, 109, 17567.
- Y. Yu-Fei, Y. Jin-Long, P. Feng, C. Yi, Chinese J. Struc. Chem. 2020, 39, 16.
- Q. Run-Zhi, W. Yan, Z. Qing-He, Y. Kai, P. Feng, Chinese J. Stru. Chem. 2020, 39, 605.
- 133. M. Li, C. Wang, Z. Chen, K. Xu, J. Lu, Chem. Rev. 2020, 120, 6783.
- 134. Y. Yamada, A. Yamada, J. Electrochem. Soc. 2015, 162, A2406.
- F. Huang, G. Ma, Z. Wen, J. Jin, S. Xu, J. Zhang, J. Mater. Chem. A 2018, 6, 1612.
- 136. N. Piao, L. Wang, X. He, J. Electrochem. Soc. 2021, 168, 030509.
- Y. Yamada, J. Wang, S. Ko, E. Watanabe, A. Yamada, *Nat. Energy* 2019, 4, 269.
- S. Perez Beltran, X. Cao, J.-G. Zhang, P. B. Balbuena, *Chem. Mater.* 2020, 32, 5973.
- D.-J. Yoo, S. Yang, K. J. Kim, J. W. Choi, Angew. Chem. Int. Ed. 2020, 59, 14869.
- 140. S. Lin, H. Hua, Z. Li, J. Zhao, ACS Appl. Mater. Inter. 2020, 12, 33710.
- A. Ramanujapuram, D. Gordon, A. Magasinski, B. Ward, N. Nitta, C. Huang, G. Yushin, *Energy Environ. Sci.* 2016, 9, 1841.
- P. Jaumaux, X. Yang, B. Zhang, J. Safaei, X. Tang, D. Zhou, C. Wang,
 G. Wang, *Angew. Chem. Int. Ed.* **2021**, *60*, 19965.
- 143. K. Xu, C. Wang, Nat. Energy 2016, 1, 16161.
- 144. D. Lin, Y. Liu, Y. Cui, Nat. Nanotech. 2017, 12, 194.
- 145. Y. Kim, D. Koo, S. Ha, S. C. Jung, T. Yim, H. Kim, S. K. Oh, D.-M. Kim, A. Choi, Y. Kang, K. H. Ryu, M. Jang, Y.-K. Han, S. M. Oh, K. T. Lee, ACS Nano 2018, 12, 4419.
- 146. H. Wu, Y. Cao, L. Geng, C. Wang, Chem. Mater. 2017, 29, 3572.
- 147. J. Zheng, P. Yan, D. Mei, M. H. Engelhard, S. S. Cartmell, B. J. Polzin, C. Wang, J.-G. Zhang, W. Xu, Adv. Energy Mater. 2016, 6, 1502151.
- 148. N. Piao, S. Liu, B. Zhang, X. Ji, X. Fan, L. Wang, P.-F. Wang, T. Jin, S.-C. Liou, H. Yang, J. Jiang, K. Xu, M. A. Schroeder, X. He, C. Wang, ACS Energy Lett. 2021, 6, 1839.
- 149. X. Ren, L. Zou, S. Jiao, D. Mei, M. H. Engelhard, Q. Li, H. Lee, C. Niu, B. D. Adams, C. Wang, J. Liu, J.-G. Zhang, W. Xu, ACS Energy Lett. 2019, 4, 896.
- Y. Yu, G. Huang, J.-Y. Du, J.-Z. Wang, Y. Wang, Z.-J. Wu, X.-B. Zhang, Energy Environ. Sci. 2020, 13, 3075.

- M. Wang, L. Huai, G. Hu, S. Yang, F. Ren, S. Wang, Z. Zhang,
 Z. Chen, Z. Peng, C. Shen, D. Wang, J. Phys. Chem. C 2018, 122,
 9825.
- G. Jiang, F. Li, H. Wang, M. Wu, S. Qi, X. Liu, S. Yang, J. Ma, Small Structures 2021, 2, 2000122.
- 153. S. Jiao, X. Ren, R. Cao, M. H. Engelhard, Y. Liu, D. Hu, D. Mei, J. Zheng, W. Zhao, Q. Li, N. Liu, B. D. Adams, C. Ma, J. Liu, J.-G. Zhang, W. Xu, *Nat. Energy* 2018, *3*, 739.
- 154. J. Zheng, G. Ji, X. Fan, J. Chen, Q. Li, H. Wang, Y. Yang, K. C. DeMella, S. R. Raghavan, C. Wang, Adv. Energy Mater. 2019, 9, 1803774.
- X. Xing, Y. Li, X. Wang, V. Petrova, H. Liu, P. Liu, *Energy Storage Mater.* 2019, 21, 474.
- J. Alvarado, M. A. Schroeder, M. Zhang, O. Borodin, E. Gobrogge, M. Olguin, M. S. Ding, M. Gobet, S. Greenbaum, Y. S. Meng, K. Xu, *Mater. Today* 2018, 21, 341.
- L.-L. Jiang, C. Yan, Y.-X. Yao, W. Cai, J.-Q. Huang, Q. Zhang, *Angew. Chem. Int. Ed.* 2021, 60, 3402.
- 158. H. Jia, L. Zou, P. Gao, X. Cao, W. Zhao, Y. He, M. H. Engelhard, S. D. Burton, H. Wang, X. Ren, Q. Li, R. Yi, X. Zhang, C. Wang, Z. Xu, X. Li, J.-G. Zhang, W. Xu, *Adv. Energy Mater.* **2019**, *9*, 1900784.
- Z.-h. Chang, J.-t. Wang, Z.-h. Wu, M. Gao, S.-j. Wu, S.-g. Lu, Chem-SusChem 2018, 11, 1787.
- 160. H. Jia, Y. Xu, S. D. Burton, P. Gao, X. Zhang, B. E. Matthews, M. H. Engelhard, L. Zhong, M. E. Bowden, B. Xiao, K. S. Han, C. Wang, W. Xu, ACS Appl. Mater. Inter. 2020, 12, 54893.
- S. Chae, W.-J. Kwak, K. S. Han, S. Li, M. H. Engelhard, J. Hu, C. Wang, X. Li, J.-G. Zhang, ACS Energy Lett. 2021, 6, 387.
- S. Hou, X. Ji, K. Gaskell, P. Wang, L. Wang, J. Xu, R. Sun, O. Borodin, C. Wang, *Science* 2021, 374, 172.

AUTHOR BIOGRAPHIES



Jiangtao Hu received his Ph.D. degree in 2018 from Peking University (China) under the supervision of Prof. Feng Pan. Between 2018 and 2021, he worked with Jie Xiao in Pacific Northwest National Laboratory (PNNL, USA) as a postdoc research fellow. Dr. Hu is currently an associate professor at the College

of Chemistry and Environmental Engineering, Shenzhen University. His research interests mainly lie in design and

development of functional materials for energy storage and conversion applications such as Li-ion battery and Na-ion battery.



Luyi Yang received his B.S. degree from the Department of Chemistry at Xiamen University (China) in 2010, and earned Ph.D. degree from the School of Chemistry at Southampton University (UK) in 2015 under the supervision of Prof. John Owen. Dr. Yang is currently a

research associate professor at the School of Advanced Materials, Peking University Shenzhen Graduate School. His research interests mainly focus on the investigation of key materials in lithium batteries.



Feng Pan, chair-professor, founding dean of the School of Advanced Materials, Peking University Shenzhen Graduate School, director of the National Center of Electric Vehicle Power Battery and Materials for International Research, received his

B.S. degree from the Department of Chemistry, Peking University in 1985 and Ph.D. from the Department of P&A Chemistry, University of Strathclyde, UK with "Patrick D. Ritchie Prize" for the best Ph.D. in 1994. Prof. Pan has been engaged in fundamental research of structure chemistry, exploring "Material Gene" for Li-ion batteries and developing novel energy conversion-storage materials and devices. He also received the 2018 ECS Battery Division Technology Award.

How to cite this article: J. Hu, Y. Ji, G. Zheng, W. Huang, Y. Lin, L. Yang, F. Pan, *Aggregate* **2022**, *3*, e153. https://doi.org/10.1002/agt2.153